PLOS BIOLOGY

RESEARCH ARTICLE

Structure of G protein-coupled receptor GPR1 bound to full-length chemerin adipokine reveals a chemokine-like reverse binding mode

Aijun Liu[1,2☯], Yezhou Liu[1☯], Geng Chen[1☯], Wenping Lyu[3☯], Fang Ye[1], Junlin Wang[1], Qiwen Liao[1], Lizhe Zhu[3]*, Yang Du[1]*, Richard D. Ye[1,4]*

1 Kobilka Institute of Innovative Drug Discovery, School of Medicine, The Chinese University of Hong Kong, Shenzhen, China, **2** Dongguan Songshan Lake Central Hospital, Dongguan Third People's Hospital, The Affiliated Dongguan Songshan Lake Central Hospital, Guangdong Medical University, Dongguan, China, **3** Warshel Institute for Computational Biology, School of Medicine, The Chinese University of Hong Kong, Shenzhen, China, **4** The Chinese University of Hong Kong, Shenzhen Futian Biomedical Innovation R&D Center, Shenzhen, China

☯ These authors contributed equally to this work.
* zhulizhe@cuhk.edu.cn (LZ); yangdu@cuhk.edu.cn (YD); richardye@cuhk.edu.cn (RDY)

Citation: Liu A, Liu Y, Chen G, Lyu W, Ye F, Wang J, et al. (2024) Structure of G protein-coupled receptor GPR1 bound to full-length chemerin adipokine reveals a chemokine-like reverse binding mode. PLoS Biol 22(10): e3002838. https://doi.org/10.1371/journal.pbio.3002838

Academic Editor: Raimund Dutzler, University of Zurich, SWITZERLAND

Received: February 28, 2024

Accepted: September 9, 2024

Published: October 28, 2024

Data Availability Statement: Underlying data can be found in the S1_Data file and the MD simulations data have been deposited in the Zenodo database (DOI 10.5281/zenodo.13711859). The density maps and the atomic coordinates for the C9-GPR1-Gi and chemerin-GPR1-Gi complex in this study have been deposited in the Electron Microscopy Data Bank (EMDB entry ID EMD-36364 and EMD-38328) and the Protein Data Bank (PDB entry ID 8JJP and 8XGM).

Abstract

Chemerin is an adipokine with chemotactic activity to a subset of leukocytes. Chemerin binds to 3 G protein-coupled receptors, including chemokine-like receptor 1 (CMKLR1), G protein-coupled receptor 1 (GPR1), and C-C chemokine receptor-like 2 (CCRL2). Here, we report that GPR1 is capable of Gi signaling when stimulated with full-length chemerin or its C-terminal nonapeptide (C9, YFPGQFAFS). We present high-resolution cryo-EM structures of Gi-coupled GPR1 bound to full-length chemerin and to the C9 peptide, respectively. C9 insertion into the transmembrane (TM) binding pocket is both necessary and sufficient for GPR1 signaling, whereas the full-length chemerin uses its bulky N-terminal core for interaction with a β-strand located at the N-terminus of GPR1. This interaction involves multiple β-strands of full-length chemerin, forming a β-sheet that serves as a "lid" for the TM binding pocket and is energetically expensive to remove as indicated by molecular dynamics simulations with free energy landscape analysis. Combining results from functional assays, our structural model explains why C9 is an activating peptide at GPR1 and how the full-length chemerin uses a "two-site" model for enhanced interaction with GPR1.

Introduction

Chemerin is a small protein encoded by the retinoic acid receptor responder 2 (*RARRES2*) gene. Chemerin is mainly expressed in adipose tissue, liver, lung, and skin [1–3]. The role of chemerin was initially identified as a chemoattractant of inflammatory cells following its discovery in psoriasis samples [4]. Chemerin was subsequently found to act as an adipokine [1,2,5,6]. Chemerin secretion and processing requires the removal of the N-terminal signaling

Funding: This work was supported by Shenzhen Science and Technology Program Grant No. RCBS20221008093330067 (AL), by grants from the Science, Technology and Innovation Commission of Shenzhen Municipality GXWD20201231105722002-20200831175432002 (RDY, YD and LZ), JCYJ20200109150019113 (YD, GC), JCYJ20200109150003938 (LZ), RCYX20200714114645019 (LZ). This work was also supported by the National Natural Science Foundation of China (grant number: 82402140 (AL), 31971179 (LZ), 32271263 (YD) and 32070950 (RDY)), China Postdoctoral Science Foundation 2022M713049 (AL) and 2021M703092 (JW), the Shenzhen-Hong Kong Cooperation Zone for Technology and Innovation (HZQB-KCZYB-2020056), the Ganghong Young Scholar Development Fund (RDY), the Start-up funds from Dongguan Songshan Lake Central Hospital (AL), the Kobilka Institute of Innovative Drug Discovery at The Chinese University of Hong Kong, Shenzhen (YD, RDY). The funders had no role in study design, data collection and analysis, decision to publish, or preparation of the manuscript.

Competing interests: The authors have declared that no competing interests exist.

Abbreviations: BRIL, b(562)RIL; CCRL2, C-C chemokine receptor-like 2; CHS, cholesteryl hemisuccinate; CMKLR1, chemokine-like receptor 1; COM, center-of-mass; CRS, chemokine recognition site; DDM, dodecylmaltoside; DNGαi1, dominant negative Gαi1; GPR1, G protein-coupled receptor 1; HRV-3C, human rhinovirus 14 3C; LMNG, lauryl maltose neopentyl glycol; MD, molecular dynamics; RARRES2, retinoic acid receptor responder 2; SAR, structure-activity relationship; TICA, time-lagged independent component analysis; TM, transmembrane; TR-FRET, time resolved-fluorescence resonance energy transfer; WT, wild type.

peptide of 20 amino acids, resulting in pro-chemerin (amino acids 21–163) with low biological activity. Further proteolytic removal of 6 amino acids from the C-terminus (158–163) leads to chemerin21-157 with full bioactivity [7]. The C-terminal synthetic fragment of human chemerin (149–157, C9) shows comparable biological activity to chemerin21-157 [8–10].

To date, 3 chemerin receptors have been identified, namely, chemokine-like receptor 1 (CMKLR1), G protein-coupled receptor 1 (GPR1), and C-C chemokine receptor-like 2 (CCRL2) [11,12]. CMKLR1 responds to chemerin and C9 peptide with activation of the Gi protein pathway and the β-arrestin pathway. In contrast, CCRL2 binds chemerin but does not mediate transmembrane (TM) signaling [4]. The biological functions of GPR1 as a chemerin receptor remain unclear. GPR1 was initially identified as an orphan receptor [13]. It was subsequently found as a chemerin receptor with uncharacterized pharmacological properties. Using a reporter assay (TANGO) for measurement of β-arrestin activation, Barnea and colleagues found that GPR1 can be activated by chemerin but with a lower potency compared with CMKLR1 [12]. Another study showed that both CMKLR1 and GPR1 could activate the β-arrestin pathway, but the amplitude of the CMKLR1-mediated arrestin recruitment was greater [14]. In terms of G protein activation, published studies showed downstream activities of RhoA/ROCK, Gαq/11, and Gαi/o, but it was not clear which one is the dominant G protein for functional coupling [15]. Given the inconsistency of these studies and the implications of GPR1 in human immunodeficiency virus replication [16–18], glucose homeostasis, cardiovascular diseases, steroid hormone synthesis, and reproductive biology [4,19–23], it is important to further investigate the structure-function relationship of GPR1.

We recently reported the cryo-EM structure of CMKLR1-Gi complex bound to the C9 peptide of chemerin [24], which illustrates a clearly defined binding pocket for the C-terminal peptide of chemerin as well as an interface for Gi protein interaction. GPR1 and CMKLR1 share high sequence homology, but whether the binding event can be translated into G protein activation is unclear. Moreover, the structure of full-length chemerin has not been determined experimentally, nor is its interaction mode with the receptors. To this end, we have solved the cryo-EM structures of the GPR1-Gi complex bound to chemerin and its C9 peptide, respectively. Our results revealed the structural basis for GPR1-dependent Gi signaling and a chemokine-like "two-site" model of interaction between chemerin and GPR1.

Methods

Expression vector design

Human GPR1 was cloned into a pFastBac vector (Invitrogen, Carlsbad, CA) for protein expression and purification. Specifically, the coding sequence of human GPR1 was fused with an N-terminal HA signal peptide followed by a FLAG tag, a human rhinovirus 14 3C (HRV-3C) protease cleavage site (LEVLFQGP) and the thermostabilized apocytochrome b(562)RIL (BRIL) fusion protein [25]. The coding sequence of human chemerin except for the last 6 amino acids was synthesized (GENERAL BIOL) and cloned into a pFastbac vector. Human dominant negative Gαi1 (DNGαi1), generated with the G203A and A326S substitution, was cloned into a pFastBac vector. N-terminal 6×His-tagged Gβ1 and Gγ2 were cloned into a pFastBac-Dual vector. scFv16 was fused with an N-terminal GP67 signal peptide and a C-terminal 8× His tag, and the coding sequence was then cloned into a pFastBac vector.

For functional assays, the full-length human GPR1 cDNA were cloned into pcDNA3.1(+) vector (Invitrogen) with an N-terminal FLAG tag. Point mutations were introduced using homologous recombination. Two fragments of GPR1 separated at mutated positions were amplified using PCR and then assembled into precut pcDNA3.1(+) vectors using the

ClonExpress Ultra One Step Cloning Kit (Vazyme Biotech; C115). Plasmids with GPR1 mutations were confirmed by DNA sequencing (GENEWIZ).

Expression and purification of the GPR1-Gi complexes

The baculoviruses expressing GPR1, chemerin, DNGαi1, Gβ1, and Gγ2 were generated and amplified using the Bac-to-Bac baculovirus expression system. The *Sf*9 cells were cultured in SIM SF Expression Medium (Sino Biological). When the cell density reached 3.5×10^6 cells/mL (in total 2 liters), the baculoviruses (GPR1, DNGαi1, Gβ1γ2) were coexpressed in *Sf*9 cells at a ratio of 1:4:2 for the C9-GPR1-Gi complex. The baculoviruses (GPR1, chemerin, DNGαi1, Gβ1γ2) were coexpressed in Sf9 cells at a ratio of 1:2:4:2 for the chemerin-GPR1-Gi complex. After infection for 60 h, the cells were collected by centrifugation at 2,000 × *g* for 15 min and kept frozen at −80˚C before complex purification.

For the purification of C9-bound GPR1-Gi protein complexes, cell pellets from a 2-L culture were resuspended in 150 mL lysis buffer (10 mM Tris (pH 7.5), 1 mM EDTA, 2.5 μg/mL leupeptin and 160 μg/mL benzamidine, 4 μM C9 peptide and 1 mg/mL iodoacetamide) for 30 min at room temperature. The lysate was centrifuged for 15 min at 18,000 × *g*, and the pellet was homogenized in 150 mL solubilization buffer (20 mM HEPES (pH 7.5), 100 mM NaCl, 10% glycerol, 1% dodecylmaltoside (DDM), 0.1% cholesteryl hemisuccinate (CHS), 2.5 μg/mL leupeptin and 160 μg/mL benzamidine, 4 μM C9 peptide, 1 mg/mL iodoacetamde, 2 mg scFv16, 25 mU/mL apyrase) using a Dounce homogenizer. The sample was stirred for 2 h at 4˚C and then centrifuged for 30 min at 18,000 × *g* to remove the insoluble debris. The solubilized supernatant fraction was incubated with 2 mL anti-FLAG affinity resin (GenScript Biotech, Piscataway, NJ) and stirred at 4˚C for 2 h. Then, the resin was manually loaded onto a gravity-flow column and extensively washed with the FLAG wash buffer (W1: 20 mM HEPES (pH 7.5), 0.1% DDM, 0.01% CHS, 100 mM NaCl, 2 mM $CaCl_2$, 4 μM C9 peptide. W2: 20 mM HEPES (pH 7.5), 0.2% lauryl maltose neopentyl glycol (LMNG), 0.02% CHS, 100 mM NaCl, 2 mM $CaCl_2$, 4 μM C9 peptide) by mixing W1 and W2 buffer in the following ratios: 5 mL:5 mL, 2 mL:8 mL, 1 mL:9 mL, 0.5 mL:9.5 mL, 0 mL:10 mL, respectively. The GPR1-Gi complexes attached to the resin were further eluted with 10 mL elution buffer (20 mM HEPES (pH 7.5), 0.01% LMNG, 0.002% CHS, 100 mM NaCl, 4 μM C9 peptide, 5 mM EDTA, 0.2 mg/ml FLAG peptide). Eluted protein complexes were concentrated to 400 μL in an Amicon Ultra-15 Centrifugal Filter Unit (Millipore, Burlington, MA) and further subjected to a size exclusion chromatography through a Superdex 200 Increase 10/300 column (GE Healthcare Life Sciences, Sweden) equipped in an AKTA FPLC system with running buffer (20 mM HEPES (pH 7.5), 0.01% LMNG, 0.002% CHS, 100 mM NaCl, 4 μM C9 peptide). Eluted fractions containing GPR1-Gi complexes were repooled and concentrated before being flash frozen in liquid nitrogen and stored at −80˚C. The purification process of the chemerin-GPR1-Gi complex was almost identical except C9 was not added.

Expression and purification of scFv16

The antibody fragment scFv16 was expressed as a secretory protein and purified as previously described [26]. Briefly, *Trichoplusia ni* Hi5 insect cells were cultured to reach a density of 3.5×10^6 cells/mL. Cells were then infected with scFv16 baculovirus at a ratio of 1:50. After 60 h of culture, the supernatant was collected and loaded onto a Ni-NTA resin column. The column was washed with 20 mM HEPES (pH 7.5), 500 mM NaCl, and 20 mM imidazole, and then subjected to elution by 20 mM HEPES (pH 7.5), 100 mM NaCl, and 250 mM imidazole. The eluted proteins were concentrated and subjected to size-exclusion chromatography using a Superdex 200 Increase 10/300 column (GE Healthcare). Finally, the purified scFv16 protein

with a monomeric peak was concentrated and flash frozen in liquid nitrogen and stored at −80˚C for further use.

Cryo-EM sample preparation and data collection

For cryo-EM sample preparation of the C9-GPR1-Gi-scFv16 complex or chemerin-GPR1-Gi complex, UltrAuFoil Au R1.2/1.3 300-mesh grids (Quantifoil) were glow discharged in a Tergeo-EM plasma cleaner. At a concentration of around 7 mg/mL, 3 μL purified complex sample was loaded on the grid and blotted for 3 s with a blotting force of 0 and then flash-frozen in liquid ethane cooled by liquid nitrogen using Vitrobot Mark IV (Thermo Fisher Scientific, Waltham, MA). Cryo-EM data were collected at the Kobilka Cryo-EM Center of The Chinese University of Hong Kong, Shenzhen, on a 300-kV Titan Krios Gi3 microscope (Thermo Fisher Scientific). The raw movies were recorded using a Gatan K3 BioQuantum Camera at the magnification of 105,000, with a pixel size of 0.85 Å. A GIF Quantum energy filter was applied to exclude inelastically scattered electrons (Gatan) using a slit width of 20 eV. The movie stacks were acquired with a total exposure time of 2.5 s fragmented into 50 frames (0.05 s/frame). The defocus range was from −1.2 to −2.0 μm. The semiautomatic data acquisition was performed using SerialEM. A total of 3,609 image stacks were collected in 48 h for the C9-GPR1-Gi-scFv16 complex, and a total of 7,706 image stacks were collected in 72 h for the chemerin-GPR1-Gi-scFv16 complex.

Image processing and model building

Data processing was performed with cryoSPARC 3.3.1 (Structura Biotechnology, Toronto, Canada). Patch motion correction and patch CTF estimation were applied to the image stacks. For the chemerin-GPR1-Gi-scFv16 dataset, 2,232,191 particles were autopicked and subjected to 2D classification. Ab initio reconstruction was performed by selecting particles in good 2D classes. The high-quality particles were selected by multiple rounds of heterogeneous refinements. Finally, a dataset with 107,273 particles was used for non-uniform refinement and local refinement, yielding a final map with a global resolution at 3.29 Å by FSC 0.143 cutoff criterion. For the C9-GPR1-Gi-scFv16 dataset, 2,280,697 particles were autopicked. 2D classification was performed, resulting in 732,629 particles selected for ab initio reconstruction. After 3 rounds of heterogeneous refinements, a final set of 208,596 particles was exported to nonuniform refinement and local refinement, yielding a map with a global resolution of 2.90 Å.

The predicted structure GPR1 and chemerin on the AlphaFold database was used to build the initial model. The coordinates of Gi1 and scFv16 from the CMKLR1-Gi-Scfv16 complex (PDB ID: 7YKD) were applied as templates. All models were docked into the EM density map using UCSF Chimera version 1.12, followed by iterative manual building in Coot-0.9.2 and refinement in Phenix-1.18.2. The statistics of the final model were further validated by Phenix-1.18.2. Structure figures were generated by Chimera or PyMOL (Schrödinger, New York, NY). The statistics of data-collection and structure-refinement are shown in S1 Table.

Molecular modeling and molecular dynamic simulation

The protonation state of the GPR1 was assigned by the web server H++ [27] assuming pH 7.4, and charmm36m [27] force field was employed in all simulations. After energy minimization, membrane relaxation, and equilibrium simulation [28], 10 independent 1-μs long production MD simulations were carried out for C9-GPR1 and the full-length chemerin-GPR1 complexes, respectively. Fifty-thousand conformations were collected in total from the assemble of trajectories. Hydrogen bonds were identified based on cutoffs for the Donor-H···Acceptor distance

and angle. The criterion employed was angle $> 120^{\circ}$ and H···Acceptor distance < 2.5 Å in at least 10% of the trajectory.

Free energy landscape estimation by parallel bias metadynamics

The unbinding free energy landscape of the C-terminus of chemerin in C9-GPR1 and the full-length chemerin-GPR1 complexes are estimated by parallel bias metadynamics [29]. In the parrel bias metadynamics simulation of C9-GPR1, the Z-component of 3 reaction coordinates were biased: (1) the (center-of-mass (COM) distance between the C-tail residue S9 and the TM region of GPR1; (2) the COM distance between the C-tail residue F8 and the TM region of GPR1; and (3) the COM distance between the C-tail residue F8 and the core of GPR1 binding pocket. This configuration facilitated the sampling of the C-tail of the C9 peptide binding and unbinding to the core of GPR1 binding pocket, while allowing the peptide to move freely on the X-Y plane.

To simulate the full-length chemerin-GPR1, we used the same reaction coordinates as C9-GPR1 to characterize the binding of the C-terminus of chemerin. Additionally, we used 2 more groups of reaction coordinates to characterize the behavior of (1) anti-β-sheet breaking and (2) the change of the COM distance between the full-length chemerin and GPR1. An ensemble of well-tempered parallel bias metadynamics simulations with different initial gaussian height and biasing factor were launched for each system, which ensures a sufficient sampling of the unbinding process in a reasonable simulation time (μs scale). A total of 35 independent metadynamics simulations were carried out for each complex. Among these simulations, the binding and unbinding process was repeatedly sampled in 28 trajectories. The full high-dimensional free energy landscapes are obtained from reweighting the sampled conformations by using the recorded 1-D bias potentials [29]. For convenience of data visualization, we grouped the reaction coordinates and then reduced the dimension of each group of reaction coordinates to 1-D by applying time-lagged independent component analysis (TICA) with lag time of 1. For C9-GPR1 complex, the high-dimensional free energy was mapped onto two 1-D reaction coordinates: tica_Z and tica_XY. For the full-length chemerin-GPR1, the high-dimensional free energy is mapped onto four 1-D reaction coordinates: tica_Z, tica_XY, tica_BETA, and tica_COM.

G protein dissociation assay

G protein activation was tested by a NanoBiT-based G protein dissociation assay [30]. HEK293T cells were plated in a 24-well plate 24 h before transfection. Lipofectamine 3000 (Invitrogen, L3000001) transfection was performed with a mixture of 92 ng pcDNA3.1 vector encoding human GPR1 (wild type (WT)/mutants) or WT human CMKLR1 for comparison, 46 ng pcDNA3.1 vector encoding Gαi1-LgBiT, 230 ng pcDNA3.1 vector encoding Gβ1, and 230 ng pcDNA3.1 vector encoding SmBiT-Gγ2 (per well in a 24-well plate), respectively. After 24 h of incubation, the transfected cells were collected and resuspended in HBSS containing 20 mM HEPES. The cell suspension was loaded onto a 384-well culture white plate (PerkinElmer Life Sciences, Waltham, MA) at a volume of 20 μL and loaded with 5 μL of 50 μM coelenterazine H (Yeasen Biotech, Shanghai, China). After 2 h of incubation at room temperature, the baseline was measured using an Envision 2105 multimode plate reader (PerkinElmer). Then, full-length chemerin (abcam, Cambridge, UK; ab256228) or synthesized C9 peptides (China-Peptides, Shanghai, China) were added to the cells in different concentration. The ligand-induced luminescence signals were measured 15 min after ligand addition and divided by the initial baseline readouts. The fold changes of signals were further normalized to PBS-treated signal, and the values (EC_{50}) were expressed as a function of different ligand concentrations based on 3 independent experiments, each with triplicate measurements.

cAMP assay

WT human GPR1 and its mutants, or WT human CMKLR1 for comparison, were transiently expressed in HeLa cells 24 h prior to collection. The cells were resuspended in HBSS buffer plus 5 mM HEPES, 0.1% BSA (w/v) and 0.5 mM 3-isobutyl-1-methylxanthine and loaded onto 384-well plates. Different concentrations of full-length chemerin or C9 peptide were prepared with 2.5 μM forskolin in the abovementioned buffer. The cells were stimulated by the ligands and 2.5 μM forskolin for 30 min in a cell incubator. Intracellular cAMP levels were measured with the LANCE Ultra cAMP kit (PerkinElmer, TRF0263) following the manufacturer's instructions. In the measurements, signals of time resolved-fluorescence resonance energy transfer (TR-FRET) were detected by an EnVision 2105 multimode plate reader (PerkinElmer). Intracellular cAMP levels were calculated according to the TR-FRET signals of the samples and cAMP standards.

β-arrestin recruitment assay

For NanoBiT-based β-arrestin recruitment assays, HEK293T cells were seeded in a 24-well plate 24 h before transfection. Cells are cotransfected with GPR1-WT-smBiT or CMKLR1-WT-smBiT (400 ng/well) and LgBiT-β-Arr1 or LgBiT-β-Arr2 (200 ng/well) by Lipofectamine 3000 (Invitrogen) for 24 h. Cells were collected and resuspended in HBSS buffer containing 20 mM HEPES, and then 20 μL of cell suspension was loaded onto a 384-well white plate at a concentration of 2×10^4 cells/well. Test samples were further loaded with coelenterazine H to a final concentration of 10 μM. After 25-min incubation at 37˚C, the samples were measured for baseline luminescence using an Envision 2105 multimode plate reader (PerkinElmer). Different concentrations of full-length chemerin or C9 peptide were added to the wells, and the luminescence signals were detected for 30 min. The signal readouts were further normalized to PBS-treated signal, and the values (EC_{50}) were expressed as a function of different ligand concentrations based on 3 independent experiments, each with triplicate measurements.

IP1 accumulation assay

WT GPR1 and its mutants, and WT human CMKLR1 for comparison, were transiently expressed in HEK293T cells for 24 h. IP1 accumulation was tested using the IP-One Gq HTRF kit (Cisbio). The cells were resuspended in the stimulation buffer (Cisbio) and incubated with different concentrations of C9 peptide diluted in the stimulation buffer for 30 min at 37˚C. The accumulation of IP1 was further determined following the manufacturer's protocols. Fluorescence intensities were measured on an Envision 2105 multimode plate reader (PerkinElmer). Intracellular IP1 levels were calculated according to the fluorescence signals of the samples and IP1 standards.

GPR1 expression level determination by flow cytometry

HEK293T cells were transfected with FLAG-tagged WT or mutant GPR1 expression plasmids for 24 h at 37˚C. Then the cells were harvested and washed in HBSS containing 5% BSA for 3 times on ice. The cells were then incubated with a FITC-labeled anti-FLAG antibody (Sigma, Cat #F4049; 1:50 diluted by HBSS buffer) for 30 min on ice and washed with HBSS. The FITC fluorescence signals demonstrating the antibody-receptor complex on the cell surface were quantified by flow cytometry (CytoFLEX, Beckman Coulter). Relative expression levels of GPR1 mutants were represented according to the fluorescence signals.

Statistical analysis

The data were analyzed with Prism 9.5.0 (GraphPad, San Diego, CA). For dose-response analysis, the curves were plotted with the log[agonist] versus response equation (3 parameters) in the software. For cAMP, IP1, and G protein dissociation assays, data points were presented as the percentages (mean ± SEM) of the maximal response level for each sample, from at least 3 independent experiments, as indicated in figure legends. For the β-arrestin recruitment assay, data were presented as raw chemiluminescence signals (mean ± SEM) from at least 3 independent experiments. The EC_{50} values were obtained from the dose-response curves. For cell surface expression, data points were presented as the percentages (mean ± SEM) of the flow cytometry fluorescence signals of WT GPR1. For statistical comparisons, analysis of variance (ANOVA) was performed using the one-way method. A *p*-value of 0.05 or lower is considered statistically significant.

Results

GPR1 functionally couples to the Gi proteins

It has been long controversial about the downstream signaling events elicited by GPR1. We hence compared TM signaling through GPR1 and CMKLR1 by performing G protein dissociation assay monitoring dissociation of Gα from Gβγ, cAMP inhibition assay measuring Gi response, IP1 accumulation assay for Gβγ signaling, and β-arrestin recruitment assays in GPR1-expressing cells stimulated with the C9 peptide and chemerin at different concentrations. No N-terminal or C-terminal modification was applied to C9 and chemerin. Upon ligand stimulation, GPR1 elicited cAMP inhibition, although to a lesser extent than CMKLR1 (Fig 1A). In NanoBiT-based G protein dissociation assay, C9 activated GPR1 and CMKLR1 with a similar EC_{50}, although the efficacy was lower for GPR1 (Fig 1B). In IP1 accumulation assay, a higher EC_{50} with a similar amplitude was observed for GPR1 (Fig 1C). These results demonstrate Gi coupling activities of GPR1 in response to C9 and chemerin stimulation. We next examined β-arrestin recruitment. Both CMKLR1 and GPR1 preferentially recruited β-arrestin1 over β-arrestin2 (Fig 1D). However, GPR1 experienced a significantly lower efficacy for β-arrestin1 recruitment, with nearly no recruitment of β-arrestin2. Chemerin shows a higher potency than the C9 peptide for both G protein and β-arrestin responses. These findings demonstrate that GPR1 functionally couples to the Gi proteins for activation.

Cryo-EM structure of the C9-GPR1-Gi complex

Having confirmed GPR1 coupling to Gi in transfected cells, we sought to determine physical interactions between GPR1 and G proteins using purified receptor and Gi proteins. As shown in S1 Fig, complex formation was readily observed between the C9-bound GPR1, the Gi heterotrimer, and the scFv16 antibody fragment that was used for stabilization of the Gi-containing complex [31]. The cryo-EM structure of the C9-bound GPR1-Gi complex was next determined to an overall resolution of 2.90 Å (Figs 2A, 2B and S1).

The C9 peptide fit snugly in a TM pocket formed by TM2, TM3, TM4, TM6, and TM7. The N-terminal end of the peptide was barely visible when the complex was viewed from the side. Within the binding pocket, the C9 peptide assumed an "S" shape (Fig 2C and 2D). The N-terminal Y1 (corresponds to Y149 in the full-length chemerin) and F2 of the C9 peptide showed extensive hydrophobic interactions with $L186^{ECL2}$, $H273^{ECL3}$, $Y188^{ECL2}$, and $I272^{6.61}$ (Fig 2E; superscripts indicate the Ballesteros–Weinstein numbering scheme for GPCRs [32]). P3 of the C9 peptide formed polar interaction with $N189^{ECL2}$ (Fig 2D). G4 had polar interaction formed between its backbone amide group and $E269^{6.58}$ (Fig 2D). Q5 with its backbone carbonyl

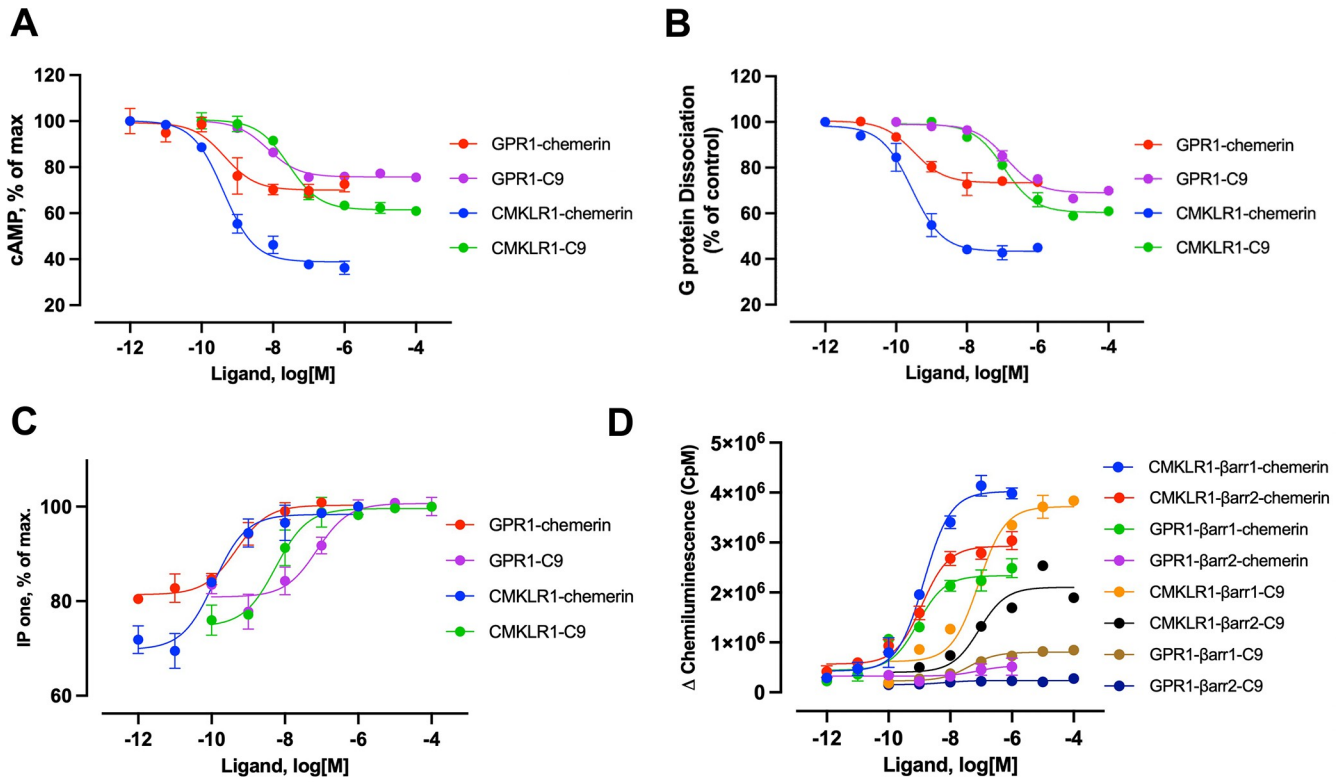

Fig 1. Gi signaling mediated by GPR1 and CMKLR1. (A) cAMP inhibition mediated by GPR1 and CMKLR1 in response to different concentrations of chemerin and C9. **(B)** G protein dissociation assay based on NanoBiT technology in transfected cells that express GPR1 and CMKLR1, respectively, and stimulated with chemerin and C9 at different concentrations. Control: HBSS without ligand addition. **(C)** IP-one accumulation in cells expressing GPR1 and CMKLR1, respectively, in response to chemerin and C9 at different concentrations. **(D)** β-arrestin recruitment upon chemerin and C9 stimulation based on NanoBiT technology, in transfected cells expressing GPR1 and CMKLR1, respectively. Data shown are means ± SEM from 3 independent experiments. The underlying data can be found in S1 Data.

https://doi.org/10.1371/journal.pbio.3002838.g001

oxygen had a polar interaction with Y96$^{2.63}$ (Fig 2D). The aromatic ring of F6 showed nonpolar interactions with F101^{ECL1} and Q283$^{7.32}$, and its backbone carbonyl oxygen had polar interaction with Y93$^{2.60}$ (Fig 2D and 2E). F8 with its aromatic ring showed extensive hydrophobic interactions with residues P287$^{7.36}$, I286$^{7.35}$, C187^{ECL2}, T290$^{7.39}$, A117$^{3.32}$, and M121$^{3.36}$ to stabilize the peptide ligand in the binding pocket (Fig 2E). S9 at the C-terminal end of the C9 peptide experienced polar interactions extensively with S114$^{3.29}$, Q118$^{3.33}$, and R176$^{4.64}$, through oxygens in its carbonyl and side chain (Fig 2D). Of note, Q$^{3.33}$ is conserved in some chemoattractant GPCRs including FPR1 and FPR2 [26,33–36], suggesting that GPR1 shares structural features in ligand binding with chemotactic peptide receptors. Previous structure-activity relationships (SARs) study has identified the importance of Y1, F2, G4, F6, and F8 for ligand activities [37], and our structural model further details the molecular interactions and rationalizes these SAR findings.

Alanine substitutions of GPR1 residues forming polar interactions with the C9 peptide including Y93$^{2.60}$, Y96$^{2.63}$, S114$^{3.29}$, Q118$^{3.33}$, R176$^{4.64}$, N189^{ECL2}, and E269$^{6.58}$, resulting in a remarkable decrease in the potency of the C9 peptide (Fig 2F–2I). Among these substituted residues, Y96$^{2.63}$A and E269$^{6.58}$A completely diminished signaling triggered by the C9 peptide. Due to extensive polar interactions between S9 in the C9 peptide and several amino acids in GPR1, single point mutations of S114$^{3.29}$, Q118$^{3.33}$, or R176$^{4.64}$ did not fully eliminate the response. This result can be explained by the flexibility at S9 where multiple hydrogen bonds

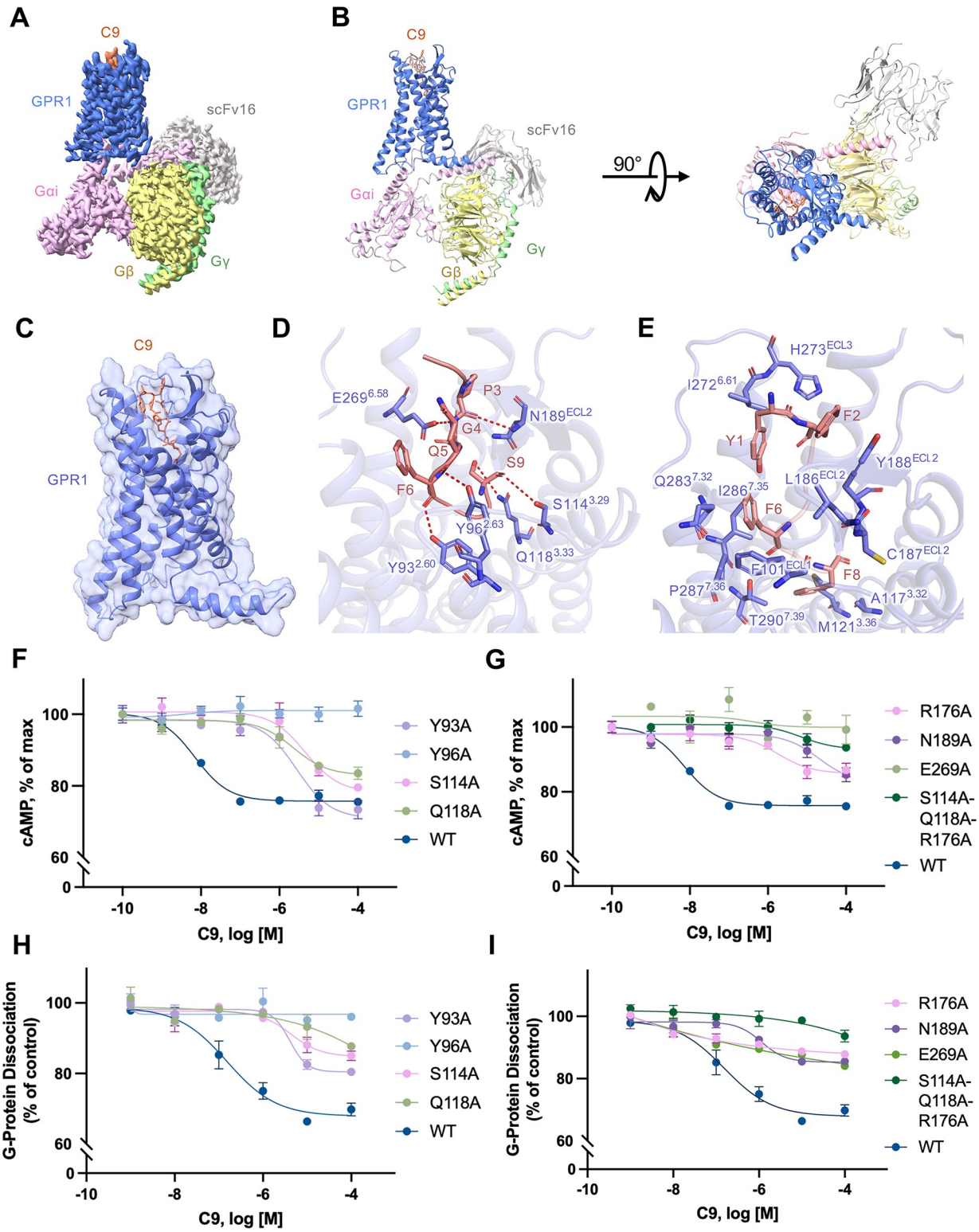

Fig 2. The structural model of C9-GPR1-Gi complex. (A) Cryo-EM density map of the C9-bound GPR1-Gi-scFv16 complex. **(B)** Overall structure of C9-GPR1-Gi-scFv16 complex from side view (left) and extracellular view (right). **(C)** Interaction between C9 and GPR1. The receptor is shown by cartoon and surface representation. C9 is shown in salmon color. **(D)** Polar interactions between C9 and GPR1. The hydrogen bonds are displayed as dashed lines. The residue numbering of GPR1 follows the Ballesteros–Weinstein nomenclature. **(E)** Nonpolar interactions between C9 and GPR1. **(F, G)** Effects of alanine substitution of selected amino acids in the C9 binding pocket on cAMP inhibition

in cells expressing the GPR1 mutants. **(H, I)** The effects on G protein dissociation of the same set of GPR1 mutants in transfected cells stimulated with different concentrations of C9. Control: HBSS without ligand addition. Data shown are means ± SEM from 3 independent experiments. The underlying data can be found in S1 Data.

https://doi.org/10.1371/journal.pbio.3002838.g002

may form dynamically between the carbonyl and side chain oxygens of S9 and S114$^{3.29}$, Q118$^{3.33}$, and R176$^{4.64}$ of GPR1. Our prediction was confirmed after introducing triple alanine substitutions at S114/Q118/R176, which completely abolished the agonist-induced cAMP inhibition and G protein dissociation upon C9 stimulation.

Cryo-EM structure of the full-length chemerin-GPR1-Gi complex

We next examined the full-length chemerin for its structure and its mode of interaction with GPR1. It is especially intriguing why, of the 137 amino acids in mature chemerin, only 9 would be sufficient for full agonistic activity. To this end, we determined the cryo-EM structure of the full-length chemerin-GPR1-Gi complex to an overall resolution of 3.29 Å (Figs 3A, 3B, S2 and S3). Except the N-terminal 15 amino acids, GPR1 in this complex is clearly defined. The majority of the full-length chemerin sits on top of the TM pocket, with interaction between the N-terminal β-strand of GPR1 and the globular core of chemerin (Fig 3B and 3C). This mode of interaction differs from most of chemokine receptors that have their N-terminal fragments wrapping around the globular core of chemokines [38,39]. Analysis of the chemerin structure, which was not experimentally determined before, identified an N-terminal α helix (H1) followed by 4 antiparallel β-strands (β1-β4) and another α helix (H2) in parallel with the β-strands (Fig 3D). The extruding C-terminus forms a C9 tail that extends deep into the TM binding pocket (red in Fig 3D). The "S-shape" of the C9 tail is clearly visible in the binding pocket similar to the C9 peptide (Fig 3E).

In the structure of the chemerin-bound GPR1, multiple binding regions are present between the chemerin ligand and the receptor. There is chemerin binding region 1 (CBR1) at the N-terminus of the receptor that interacts with the β4 strand of chemerin (Fig 4A). There is also a chemerin binding region 2 (CBR2), defined by the TM binding pocket that interacts only with the C9 tail of chemerin (Fig 4A). Detailed molecular interactions between the full-length chemerin and GPR1 were analyzed (Fig 4B). Multiple polar interactions were observed at CBR1, where S23^{NT} and E25^{NT} interact with R93 of chemerin, and S26^{NT} forms a hydrogen bond with L91 at the β4 strand of chemerin (Fig 4B). Multiple nonpolar interactions between the proximal N-terminus of GPR1 and the loop between H1 and β1 of chemerin strengthen and stabilize chemerin binding at CBR1. Like C9 interaction with the ligand binding pocket, the canonical TM binding pocket for full-length chemerin is surrounded by TM2, 3, 4, 6, and 7. These structures together form the CBR2. Multiple polar bonds are present between the chemerin C-terminal C9 tail region (126–137) and receptor CBR2 (Fig 4B). The side chain of chemerin H126 forms polar bond with I272$^{6.61}$, and Y129 interacts with E269$^{6.58}$. Similar to C9 peptide binding to GPR1, the backbone carbonyl oxygen of P131 forms hydrogen bond with N189^{ECL2}, and polar interactions are present between Q133 and Y96$^{2.63}$. F134 uses its backbone carbonyl oxygen to form polar interaction with Y93$^{2.60}$, and the C-terminal end S137 has hydrogen bond with Q118$^{3.33}$. F130 with its aromatic ring forms nonpolar interactions with V179^{ECL2}, the aromatic ring of F134 has hydrophobic interactions with F101^{ECL1} and Q283$^{7.32}$, and extensive hydrophobic interactions are present between chemerin F136 and GPR1 A117$^{3.32}$, T290$^{7.39}$, S114$^{3.29}$, and R176$^{4.64}$. Of interest, another pair of polar interactions is found between E109 of chemerin at helix H2 and H194$^{5.26}$ of GPR1 near ECL2. A similar polar interaction feature is present between some chemokines and ECL2 of the respective chemokine receptors and defined as chemokine recognition site 3 (CRS3) [38]; this region of

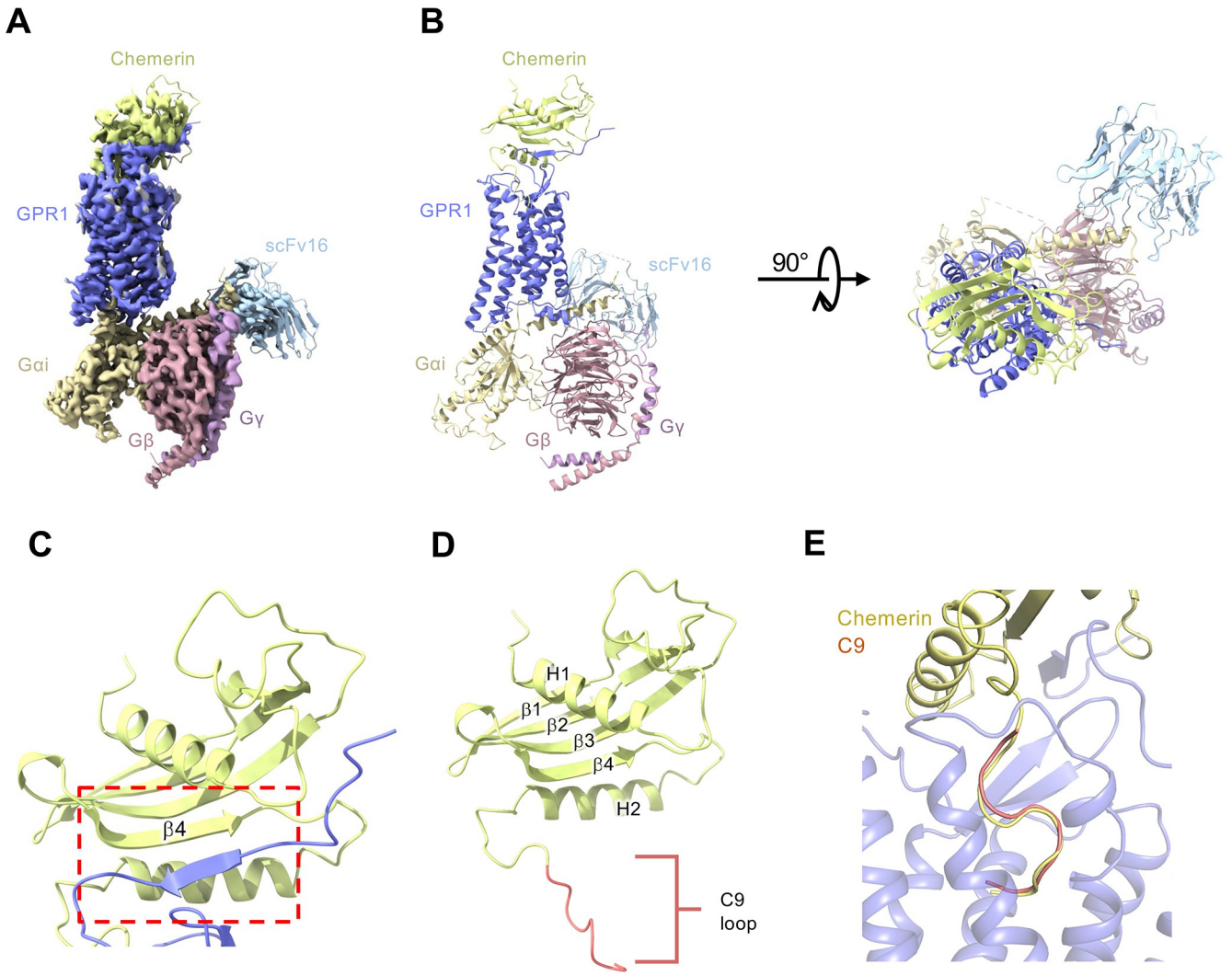

Fig 3. Overall structure of full-length chemerin-GPR1-Gi complex. (A) Cryo-EM density map of GPR1-Gi-scFv16 complex bound to chemerin. **(B)** Overall structure of full-length chemerin-GPR1-Gi-scFv16 complex from side view (left) and extracellular view (right). **(C)** Interaction between the β4 strand of chemerin (grass green) and the N-terminal β strand of GPR1 (slate blue). **(D)** Structure of full-length chemerin (21–157). Structural motifs including helices H1 and H2, β-strands β1-β4, and the C-terminal C9 tail (red). **(E)** Comparison between the binding poses of chemerin and C9 peptide in the TM pocket of GPR1. Chemerin is shown in yellow, and C9 peptide is shown in salmon.

https://doi.org/10.1371/journal.pbio.3002838.g003

GPR1 can hence be categorized into chemerin binding region 3 (CBR3). These 3 chemerin binding regions work together to stabilize receptor-chemerin interactions and activate the receptor.

Alanine substitutions of the key residues in the CBR2 binding pocket of GPR1 were performed, and the resulting receptors were expressed for functional assays including cAMP inhibition and G protein dissociation to determine any changes in GPR1 activation by the full-length chemerin (Fig 4C–4F). The EC_{50} of chemerin in eliciting cAMP inhibition and G protein dissociation was around 10^{-10} M, while for C9 peptide, the EC_{50} is 10^{-8} M. In response to chemerin binding, the $Y93^{2.60}A$ and $Q118^{3.33}A$ mutants reduced the potency by 3 magnitudes, while $Y96^{2.63}A$, $N189^{ECL2}A$, and $E269^{6.58}A$ completely abolished both cAMP inhibition and G protein dissociation. All mutants were properly expressed on the cell surface (S4 Fig), thus excluding global misfolding of the receptors after alanine substitution at these positions.

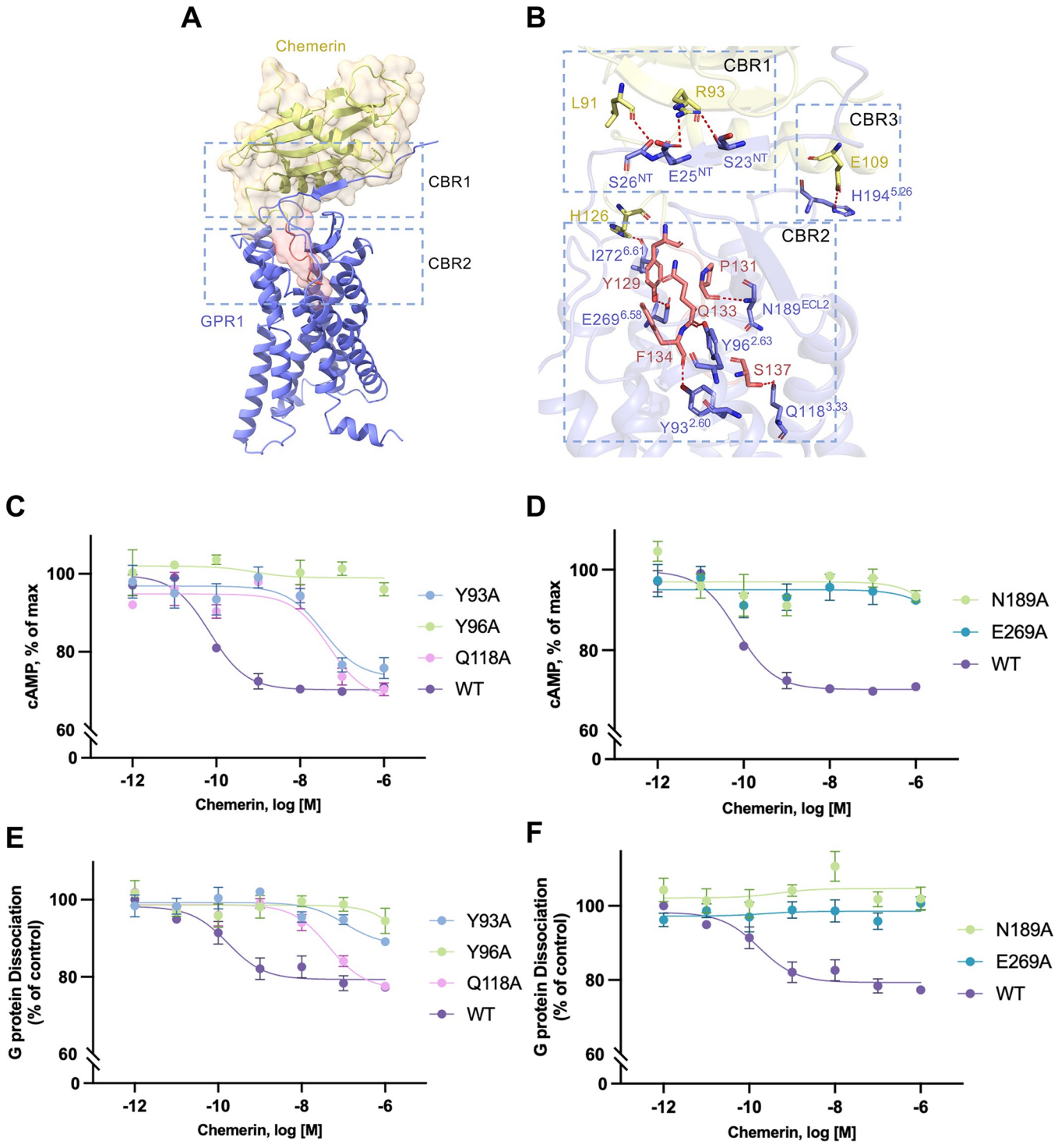

Fig 4. Ligand binding pockets in chemerin-GPR1-Gi complex. (A) Interaction between chemerin and GPR1. Chemerin is shown by cartoon and transparent surface representation. The C-terminal nonapeptide (C9) is highlighted in salmon color. **(B)** Polar interactions between chemerin and GPR1. The hydrogen bonds are displayed as dashed lines. The residue numbering of GPR1 follows the Ballesteros–Weinstein nomenclature. **(C, D)** Effects of alanine substitution of selected amino acids in the chemerin binding pocket on cAMP inhibition, in cells expressing the GPR1 mutants. **(E, F)** The effects on G protein dissociation of the same set of GPR1 mutants in transfected cells stimulated with different concentrations of chemerin. Control: HBSS without ligand addition. Data shown are means ± SEM from 3 independent experiments. The underlying data can be found in S1 Data.

https://doi.org/10.1371/journal.pbio.3002838.g004

Despite having indistinguishable postures in the CBR2 pocket, C9 and the full-length chemerin have different sidechain orientations, leading to slightly altered polar contacts with the receptor TM pocket. Altogether, these results support the role of the substituted amino acid residues of GPR1 in polar interactions with the full-length chemerin.

Thermodynamic stability of the C-terminus chemerin in GPR1 binding pocket

All-atom molecular dynamics (MD) simulations were performed for the GPR1-C9 complex and full-length chemerin-GPR1 complex at room temperature (10 replicas of 1-μs simulation), respectively. For the GPR1-C9 complex, the structure captured by cryo-EM were overall stable under thermodynamic perturbation (S5 Fig). The binding pose of the C9 peptide were well kept through the assemble of 1-μs trajectories (Figs 5, S5 and S6). Except the hydrophobic Phe (F2), all of the 9 residues in C9 peptide form hydrogen bonds (H-bonds) with GPR1 (Fig 5). The residues close to the C-terminal end of the C9 peptide formed several H-bonds with $Y96^{2.63}$, $N189^{ECL2}$, $R176^{4.64}$, $S114^{3.29}$, $Y262^{6.51}$, and $K210^{5.42}$. $N189^{ECL2}$ and $Y96^{2.63}$ also formed H-bonds with P3 and Q5 on the C9 peptide. The N-terminus of the peptide ligand was more likely to interact with negatively charged $E269^{6.58}$. The latter also interacted with G4, while the G4 formed a stable H-bond with $R176^{4.64}$ (Fig 5B). For the chemerin-GPR1 complex, hydrogen bond formation was readily observed between the C-terminus of chemerin and $Y96^{2.63}$, $N189^{ECL2}$, $R176^{4.64}$, $S114^{3.29}$, $E269^{6.58}$, and $K210^{5.42}$ of GPR1 (Fig 5C). These interactions resulted in a complex network between C9 and the receptor, which rationalized the thermodynamic stability of the C9 peptide in the binding pocket of GPR1.

Results of the MD simulations were correlated with functional assay data of the EC_{50} values of cAMP inhibition assays, using WT and alanine substituted mutants of GPR1. Alanine substitution of $N189^{ECL2}$ and $Y96^{2.63}$, which have the top occupancy scores on single H-bond (Fig 5A), abrogated cAMP inhibition ($-\log EC_{50} = 0$), indicating their functional importance. Another functionally important residue is $E269^{6.58}$, which has low single H-bond occupancy (<0.6, Fig 5A) but the highest overall H-bond occupancy (occupancy values >1.5) when all associated H-bonds were considered. Its substitution with alanine led to a loss of cAMP inhibition. Therefore, there is a high-level correlation between the polar interactions of C9-GPR1 and its functions. Compared to the C9-GPR1, the H-bond stability of the C-terminus of the full-length chemerin is overall improved: The occupancy of most H-bonds is increased, which results in an improvement of the average occupancy (highlighted by dotted lines, Fig 5A). Importantly, the residues with a stronger impact on cAMP inhibition, Y96, N189, and E269 (Fig 4C-4F), form more stable H-bonds with the full-length chemerin than with the nonapeptide C9.

The free energy landscape of unbinding of the C-terminus from the GPR1 pocket

To further compare the difference of full-length chemerin-GPR1 complex and the C9-GPR1 complex, we estimated the free energy landscape of unbinding of the C-terminus from the GPR1 pocket. An ensemble of parallel-bias metadynamics simulations were carried out for the full-length chemerin-GPR1 and C9-GPR1 complex, respectively (Figs 6 and S7–S9). Unbinding of C9 from the GPR1 binding pocket requires overcoming a free energy barrier of about 8 kCal/mol (Fig 6A) along a reaction coordinate constructed by Z-direction component of distance (tica_Z). For the full-length chemerin, the corresponding unbinding free energy barrier along tica_Z is significantly increased (>20 kCal/mol, Fig 6A). Moreover, 2 additional free energy barriers, each with a height of approximately 6.5 kCal/mol, are observed along the

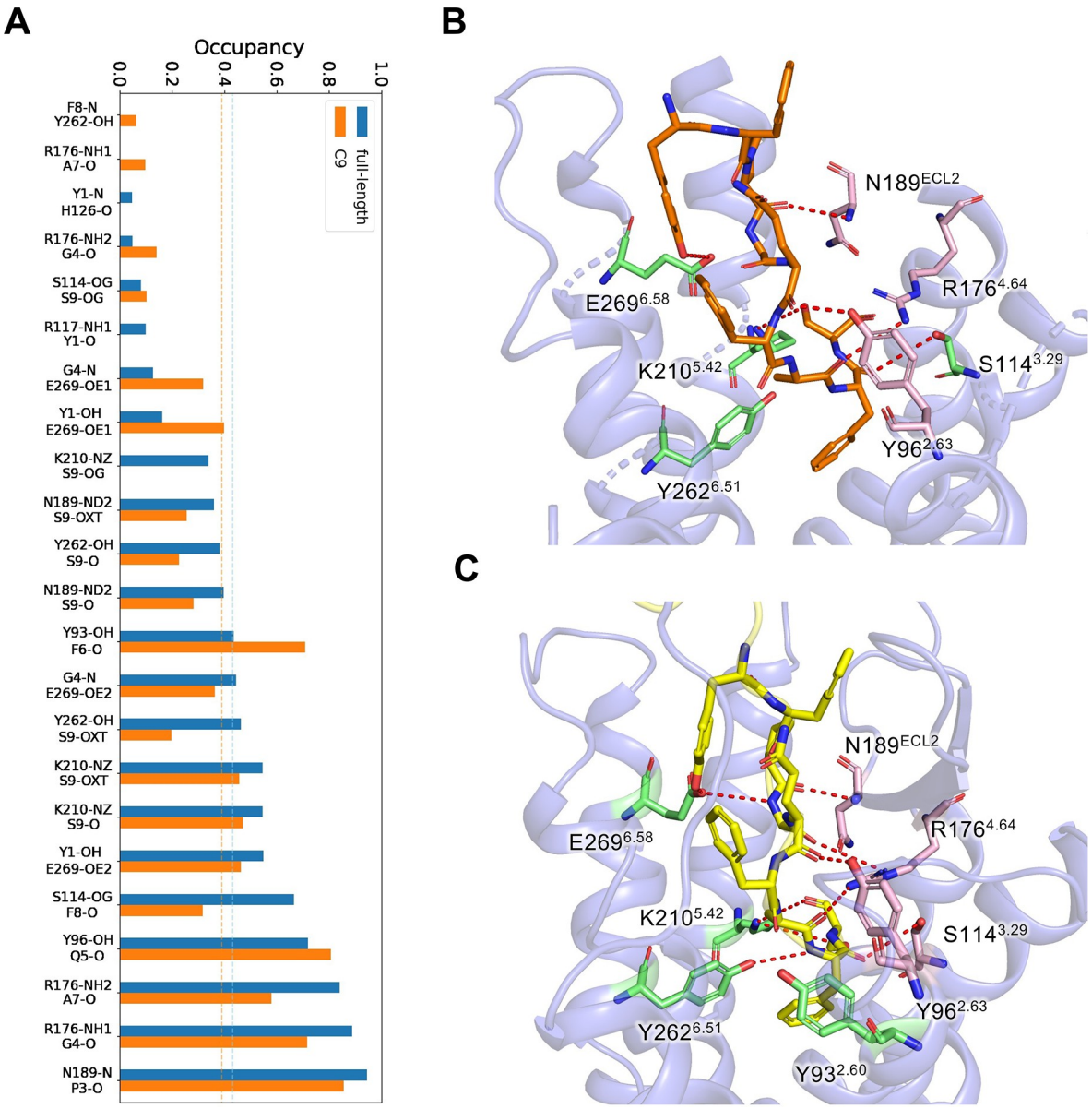

Fig 5. Thermodynamic stability analysis of the GPR1-C9 interface with μs-scale MD simulations. (A) The occupancy of all H-bonds between the C-terminus of chemerin and GPR1 (full-length) and C9 and GPR1 (C9) observed in MD simulations. The average occupancy of the 2 complexes are marked as dotted line, respectively. The underlying data can be found in S1 Data. **(B)** Side view of the distributions of functionally related residues around the C9 peptide. **(C)** Side view of the distributions of functionally related residues around the C-terminus of full-length chermerin. Hydrogen bonds are marked with red dotted lines.

https://doi.org/10.1371/journal.pbio.3002838.g005

unbinding path (tica_Z) before the C-terminus of the full-length chemerin is released (tica_Z > 2.6, Fig 6A and 6B).

As observed in the cryo-EM structures (Figs 2 and 3), the binding poses of C9 and the C-terminus of full-length chemerin are very similar, but the interaction between GPR1 and the N-terminus of full-length chemerin adds another factor for consideration. The N-terminus of full-length chemerin forms an antiparallel β-sheet with the β-strand in the N-terminus of GPR1 (Fig 3C). A projection of free energy landscape on the reaction coordinate of breaking of the antiparallel β-sheet (tica_BETA) reveals that the major energy barrier (approximately 8

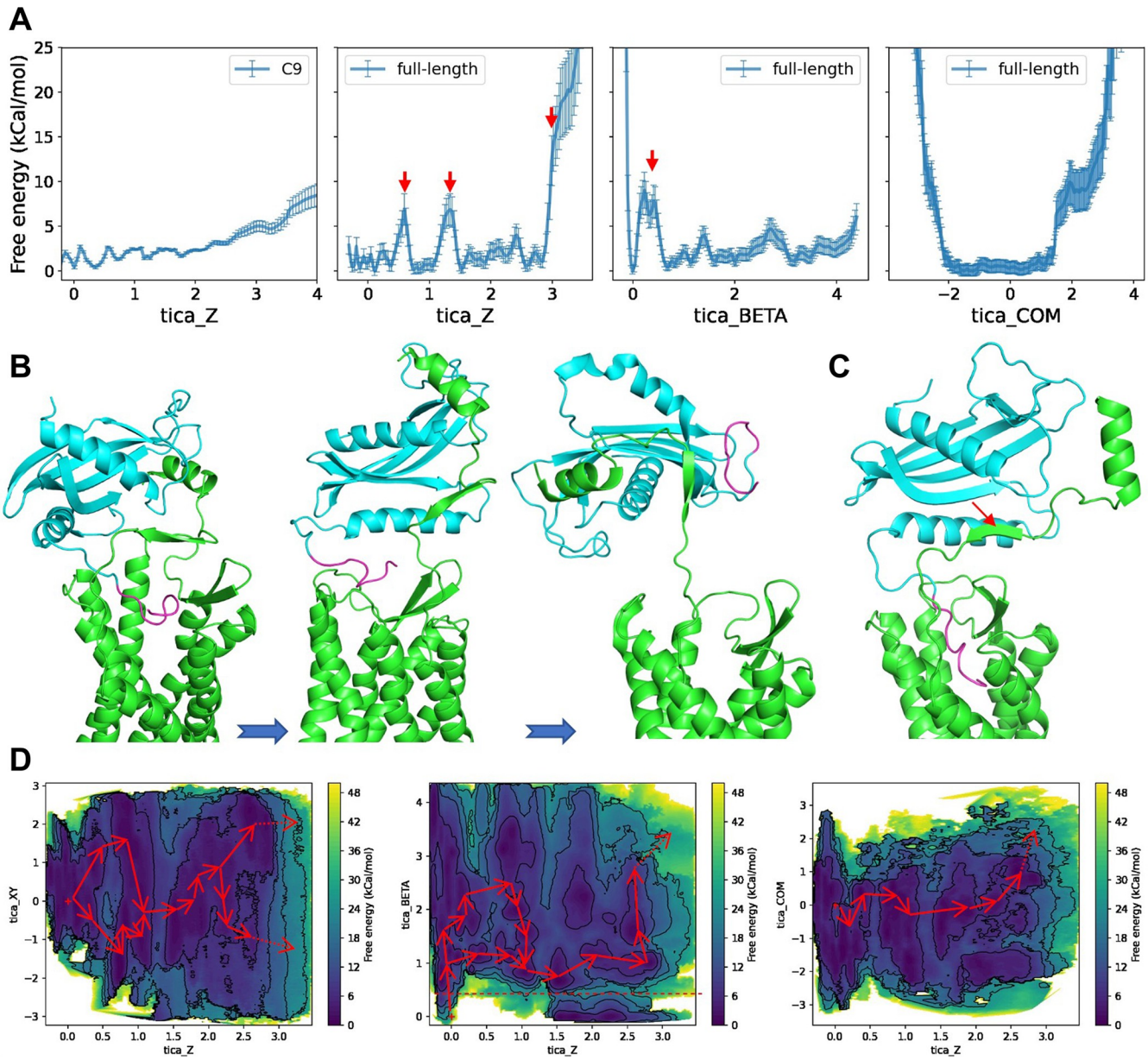

Fig 6. The free energy landscapes of unbinding the C-terminus from the GPR1 pocket. (A) 2D projection of unbinding free energy of C9-GPR1 complex (first column) and full-length chemerin-GPR1 complex (second-fourth columns). Arrows mark the high energy states of unbinding along the reaction coordinates of tica_Z and tica_BETA, respectively. **(B)** The high energy states of unbinding along the reaction coordinate tica_Z of full-length chemerin-GPR1 complex. **(C)** The high energy states of unbinding along the reaction coordinate tica_BETA of full-length chemerin-GPR1 complex. The break point of anti-β-sheet is marked with arrow. **(D)** 2D projection of unbinding free energy of full-length chemerin-GPR1 complex. Several possible unbinding pathways are marked by red arrows on the free energy map for clarity. The red dotted line marks the location of tica_BETA = 0.5 on the map. The underlying data can be found in S1 Data.

https://doi.org/10.1371/journal.pbio.3002838.g006

kCal/mol) is located very close to the starting point (tica_BETA < 1, Fig 6A and 6C). On the contrary, no significant free energy barrier is observed before the separation of full-length chemerin from GPR1 (tica_COM > 1.8, Fig 6A). These results suggest that unbinding of the C-terminus of the full-length chemerin from the GPR1 transmembrane pocket is more sensitively related to the breaking of the antiparallel β-sheet (Fig 6C). Indeed, we find that there is no path to release the C-terminus of chemerin from the GPR1 binding pocket if the

antiparallel β-sheet remains unaltered (tica_BETA < 0.5, marked with red dotted line) (Fig 6D). In other words, the formation of antiparallel β-sheet with the full-length chemerin acts as a crucial step to lock the stable binding of its C-terminus to GPR1. This effect does not exist in the interaction between C9 and GPR1.

Activation mechanism of the GPR1-Gi complex

To investigate the conformational changes associated with the activation of GPR1, we compared the structure of active GPR1 and an antagonist-bound inactive C5aR (C5aR-PMX53, PDB ID: 6C1R) for its homology to GPR1, or a C9-bound active CMKLR1 (CMKLR1-C9, PDB ID: 7YKD), respectively (Fig 7). The comparison also revealed an outward movement of TM5 and TM6, and an inward movement of TM7, in the activation of GPR1 (Fig 7A). Of note, the $D^{3.49}$-$R^{3.50}$-$Y^{3.51}$ motif found in most Class A GPCRs for G protein activation was replaced with D134-H135-Y136 in GPR1. Previous reports indicate that polar interaction of $R^{3.50}$ and $Y^{5.58}$ is important for G protein activation [24,40,41] (Fig 7B). However, the apparent activation of G proteins in GPR1, which only has $H^{3.50}$ in this motif, suggests that the $R^{3.50}$-$Y^{5.58}$ interaction is not critical to G protein activation. Supporting this notion, our substitution of $H^{3.50}$ with arginine did not significantly change G protein dissociation (Fig 9D) but made the receptor less capable of inhibiting cAMP (Fig 9A). Alanine substitution of $H^{3.50}$ led to a complete loss of function (Fig 9A and 9D). These results indicate that the $D^{3.49}$-$H^{3.50}$-$Y^{3.51}$ motif in

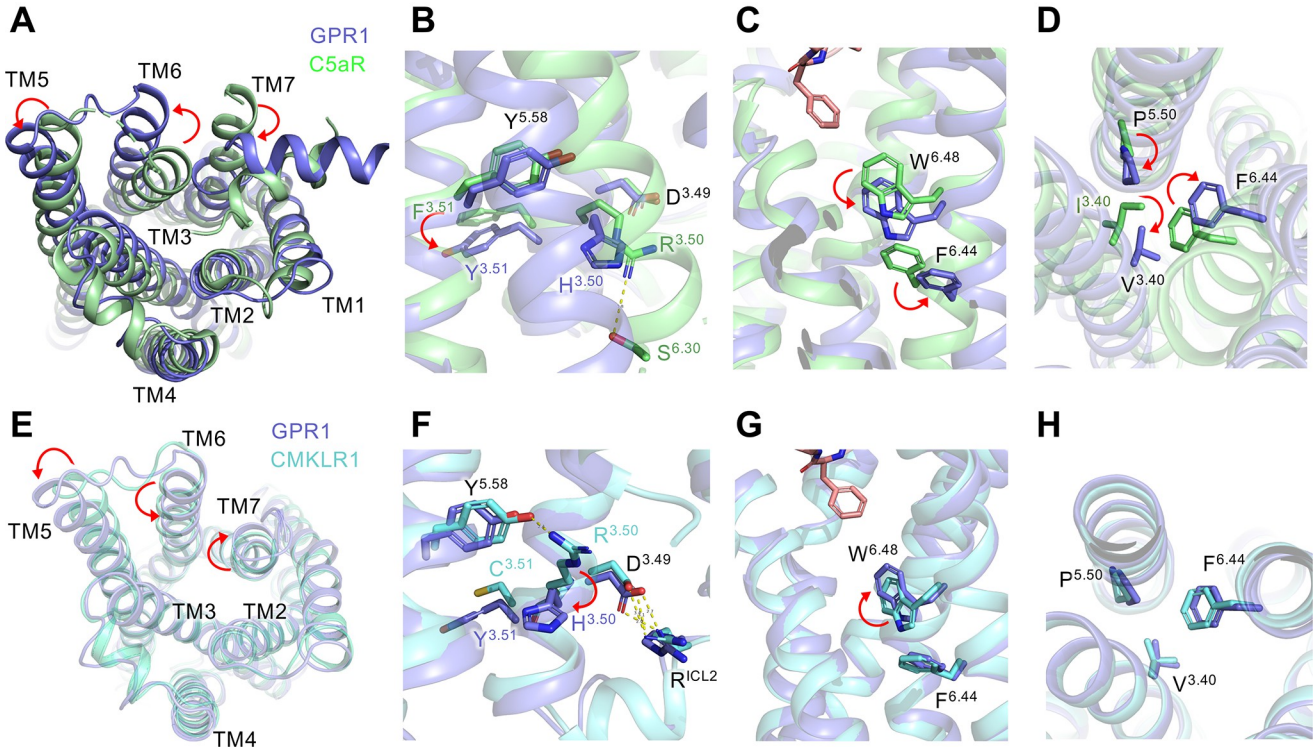

Fig 7. Comparison of GPCR structural motifs for G protein activation. **(A)** Intracellular view of the movement of GPR1 TM helix 5, 6, and 7 (shown in marine blue) in comparison with inactive C5aR (PDB ID: 6C1R, shown in lime green). **(B)** Side close-up view of the $D^{3.49}$-$R^{3.50}$-$Y^{3.51}$ motif. A downward movement of $Y^{3.51}$ of GPR1 is highlighted by a red arrow. **(C)** Side close-up view of the "toggle switch," $W^{6.48}$ and $F^{6.44}$, an anticlockwise rotation is highlighted for GPR1. **(D)** Rotamer conformational changes at the $P^{5.50}$-$I/V^{3.40}$-$F^{6.44}$ motif of GPR1 and C5aR, respectively. **(E)** Intracellular view of the movement of GPR1 TM helix 5, 6, and 7 (shown in marine blue) in comparison with active CMKLR1 (PDB ID: 7YKD, shown in cyan). **(F)** Side close-up view of the $D^{3.49}$-$R^{3.50}$-$Y^{3.51}$ motif. A downward movement of $H^{3.50}$ of GPR1 is highlighted by a red arrow. **(G)** Side close-up view of the "toggle switch," $W^{6.48}$ and $F^{6.44}$, a clockwise rotation is highlighted for GPR1. **(H)** No significant conformational change at $P^{5.50}$-$I/V^{3.40}$-$F^{6.44}$ motif of GPR1 and CMKLR1, respectively.

https://doi.org/10.1371/journal.pbio.3002838.g007

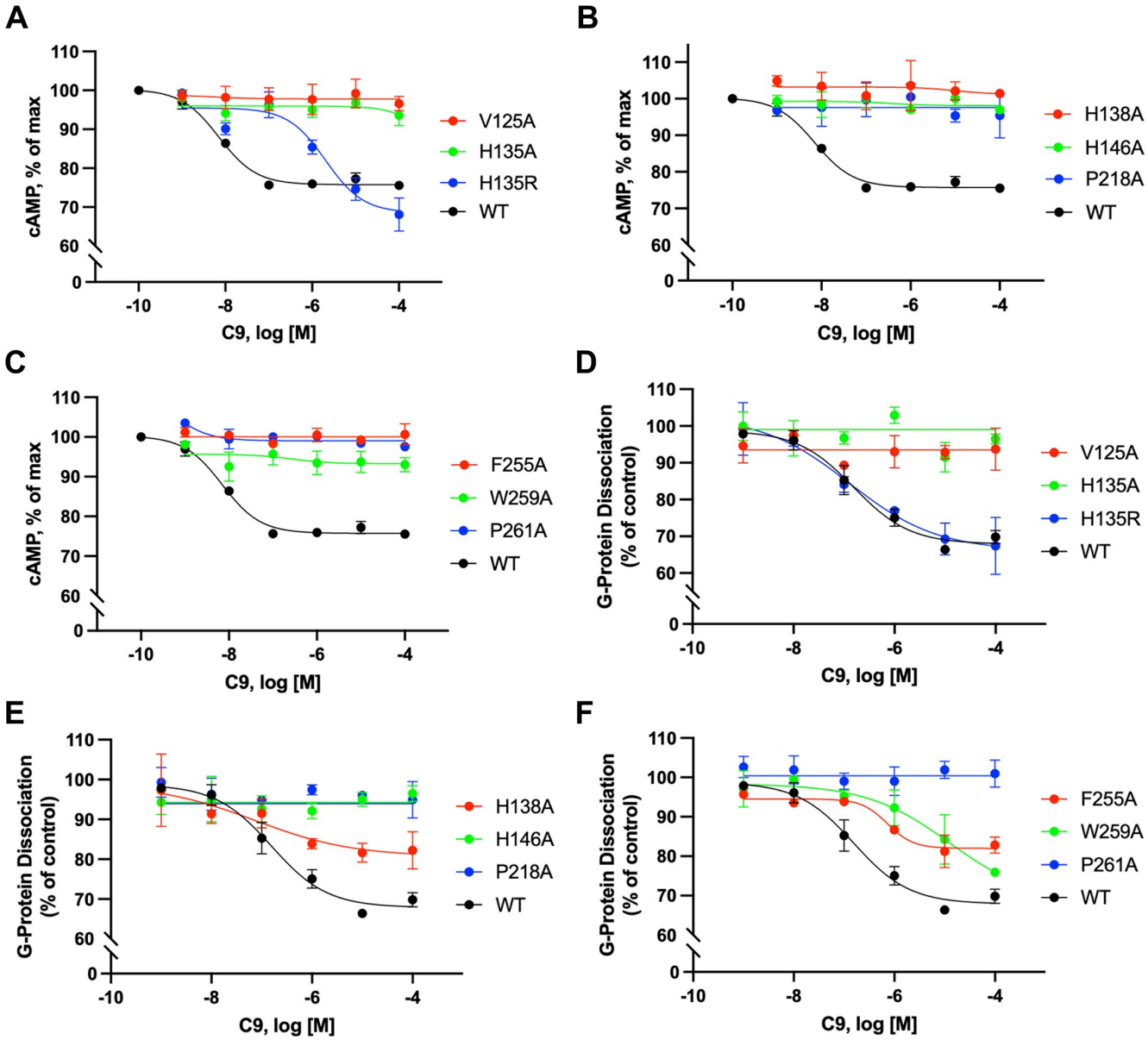

Fig 9. Point mutations at key residues for G protein activation affect cAMP inhibition and G protein dissociation. (A–C) cAMP response in HeLa cells transfected to express WT or mutant GPR1. Different concentrations of C9 are applied. **(D–F)** G protein dissociation in HEK293T cells cotransfected to express WT or mutant GPR1, Gαi1-LgBiT, Gβ1, and SmBiT-Gγ2. Different concentrations of C9 are applied. Control: HBSS without ligand addition. All data shown are means ± SEM from 3 independent experiments. The underlying data can be found in S1 Data.

https://doi.org/10.1371/journal.pbio.3002838.g009

the context of the overall sequence of GPR1 remains functional in G protein activation, even in the absence of an $R^{3.50}$-$Y^{5.58}$ interaction.

The highly conserved residue $W259^{6.48}$ as a "toggle switch" of G protein activation showed a downward rotation in the GPR1 structure (Fig 7C), which is characteristic in other activated GPCRs [40,41]. For the $P^{5.50}$-$I/V^{3.40}$-$F^{6.44}$ motif, rotamer conformational changes were displayed in GPR1 in comparison with the inactive C5aR (Fig 7D). To further identify the structural basis for different signaling of GPR1 and CMKLR1 upon activation, we compared active structures of the 2 receptors. The C9 peptide ligand was found to have an average of 1.2 Å upward shift away from the "toggle switch" $W259^{6.48}$ in GPR1, and the residues in contact with

the ligand were closer to the extracellular loop of GPR1 than CMKLR1 (S10 Fig). An outward movement of TM5, TM7, and an inward movement of TM6 was demonstrated in both receptors from inactive states to active states (Fig 7E). As for the DRY motif, CMKLR1 presents a DRC in position and $R^{3.50}$ formed a polar interaction with the $Y^{5.58}$ residue (Fig 7F). $H135^{3.50}$ in GPR1, however, pointed to the cytosolic direction with no observable polar interaction with adjacent receptor residues. For the "toggle switch," $W259^{6.48}$ in GPR1 shifted slightly upwards (Fig 7G). There is not much difference observed in the orientation of the $P218^{5.50}$-$V125^{3.40}$-$F255^{6.44}$ motif (Fig 7H). For residues lining all these examined motifs, the orientation and geometry of side chains in the chemerin-bound GPR1 and C9-bound GPR1 are the same (S11 Fig). Overall, despite differences in the geometry and important motifs between GPR1 and CMKLR1, GPR1 is able to activate the Gi proteins albeit with a lower amplitude.

Next, the interaction between an activated GPR1 and the Gi class of heterotrimeric G proteins was examined. In this study, we adopted DNGαi1, a dominant negative form of human Gαi1 containing the G203A and A326S mutations for decreased affinity for nucleotide binding and increased stability of heterotrimeric G protein complex [42,43]. In the structure, the α5 helix of Gαi inserts into the intracellular binding cavity of GPR1, forming hydrophobic interactions with $F76^{2.43}$, $L151^{4.39}$, $V251^{6.40}$, $Y226^{5.58}$, $T247^{6.36}$, and $K310^{8.49}$ (Fig 8A). Of note, some polar interactions are found between α5 helix G352 and GPR1 $H135^{3.50}$, α5 helix N347 and GPR1 $H138^{3.53}$, and αN helix R32 and GPR1 $H146^{ICL2}$ (Fig 8A). All residues of GPR1 accommodating Gα binding share the same side chain geometry, implying the conservation of structure in G protein activation by different ligands (S11 Fig). Additionally, we also observed a hydrogen bond between GPR1 helix 8 and D312 of the Gβ subunit (Fig 8B).

The interaction between the heterotrimeric Gi protein and the receptor was next compared with several Gi-coupled GPCRs, including the active CMKLR1 and CCR5 (PDB ID: 7F1R), and the inactive C5aR and CXCR4 (PDB ID: 3ODU) (Fig 8C–8E). The orientation of TM6 and TM7 marks the most remarkable difference between active and inactive receptors (Fig 8C and 8D). For the active receptors GPR1, CMKLR1, and CCR5, TM6 displays an outward tilt allowing space for an interface between the receptor and the C-terminal α5 helix of Gαi (Fig 8C). Helix 8 of the active receptors shows a movement to the intracellular compartment for engagement of the Gβ subunit (Fig 8C). An inward movement of TM7 is also observed for GPR1 and other active receptors compared with the inactive representatives (Fig 8D). Although we did not observe much polar interaction between GPR1 and the αN helix of Gαi as in CMKLR1 [24], the αN helix of Gαi has moved upwards for closer proximity with the receptor helix 8 (Fig 8E). These features contribute to the activation of G protein by GPR1.

We verified the proposed mechanisms of G protein activation by introducing point mutations to the key residues. In addition to the substitution of $H135^{3.50}$ into the canonical arginine, as mentioned above and shown in Fig 9A, point mutations of $P218^{5.50}$-$V125^{3.40}$-$F255^{6.44}$ into alanine greatly reduced the cAMP inhibition as well as G protein dissociation (Fig 9). Substitution of the "toggle switch" $W259^{6.48}$ with alanine caused a complete loss in cAMP inhibition, yet G protein dissociation was partially retained with a decreased efficacy and potency (Fig 9C and 9F). For the interaction interface between the receptor and Gαi, alanine substitution at $H135^{3.50}$, $H138^{3.53}$, and $H146^{ICL2}$ completely diminished G protein dissociation and cAMP inhibition (Fig 9A, 9B, 9D and 9E). All these functional data confirmed the importance of the aforementioned key residues in activating Gi proteins.

Discussion

There is increasing awareness of the importance of chemerin in immune regulation and lipid biogenesis, which are biological processes associated with a number of common illnesses

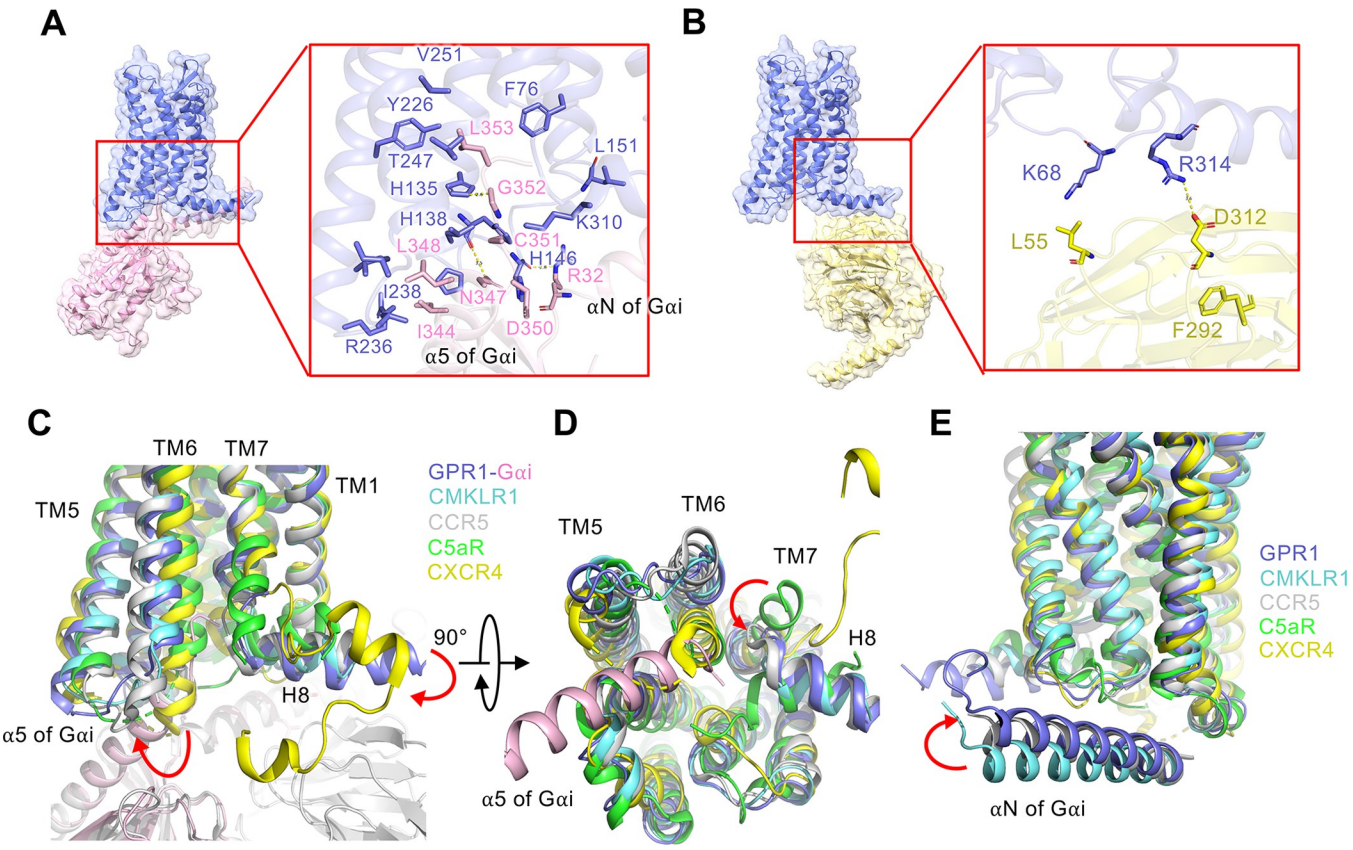

Fig 8. G protein interface of the C9-bound GPR1-Gi complex. (A) The interactions between the α5 helix of Gαi (pink) and GPR1 (marine blue) in the cavity at ICL3, TM5, TM6, and TM7 regions. **(B)** The interactions between Gβ subunit (yellow) and H8 of the receptor (marine blue). **(C)** Comparisons of the interactions between the α5 helix of Gαi and TM5, TM6, and ICL3 of several Gi-coupled receptors including GPR1 (marine blue), CMKLR1 (cyan, PDB ID: 7YKD), CCR5 (gray, PDB ID: 7F1R), C5aR (lime green, PDB ID: 6C1R), and CXCR4 (yellow, PDB ID: 3ODU). **(D)** 90˚orientation of (C) for intracellular view showing the locations of ICL2, ICL1, and H8. **(E)** Same as (C) and (D), yet the interactions of the αN helix of Gαi with these receptors are compared.

https://doi.org/10.1371/journal.pbio.3002838.g008

including acute inflammation, psoriasis, angiogenesis, obesity, diabetes, nonalcoholic fatty liver disease, ovarian cancer, and endometrial cancer [4–6,20]. It is therefore necessary to understand how chemerin exerts these physiological and pathological functions through the chemerin receptors. Of the 3 chemerin receptors identified, CMKLR1 is well known for mediating most biological activities of chemerin, and CCRL2 is a nonfunctional chemerin receptor serving as a scavenger [4]. In comparison, the functions of GPR1 are less clear. Initially identified as an orphan receptor [13], the natural ligand of GPR1 was not clear until 2008, when Barnea and colleagues reported chemerin-induced membrane association of β-arrestin2 using a functional assay for protein-protein interaction [12]. Chemerin was more potent on GPR1 (EC_{50} of 240 pM) than on CMKLR1 (3 nM) in β-arrestin2 recruitment in this assay. The same also applied to the C9 peptide, which showed a higher potency (EC_{50} of 1 nM) on GPR1 than on CMKLR1 (24 nM). Based on these results, GPR1 was considered a receptor that activates the β-arrestin2 pathway [12,44], although other studies showed its ability to mediated G protein signaling as well [14,45].

In this study, we prepared the chemerin-GPR1-Gi complex (and C9-GPR1-Gi complex) for structural studies using cryo-EM. Our findings represent the first high-resolution structure of full-length chemerin bound to GPR1, which allowed us to make comparison of this chemotactic small protein with chemokines and chemotactic peptides. Our findings also confirmed an

early prediction that chemerin acts as a "reverse chemokine" with an N-terminal core region and a C-terminal loop for receptor activation, which is the mirror image of a canonical chemokine that uses its N-terminus for receptor activation and C-terminus as core regions [46]. Another piece of evidence that supports chemerin as a chemokine-like chemoattractant [46,47] is our finding that chemerin uses a "two-site" model similar to chemokine interaction with chemokine receptors [4,48]. Notably, our cryo-EM structure of full-length chemerin-bound GPR1 Gi protein signaling complex provides direct proof for such a "two-site" model with the following features. The N-terminus of GPR1 provides CBR1, which forms multiple polar and nonpolar interactions with the cavity formed between the H2 helix and β4 sheet of chemerin and serves to stabilize chemerin binding. One important component of CBR1 is the antiparallel β-sheet in the N-terminus of GPR1 that forms an antiparallel sheet together with the β-strands of chemerin. Our metadynamics analysis shows the importance of breaking this antiparallel β-sheet before dissociation of the C-terminus of chemerin from the TM binding pocket, indicating that the antiparallel β-sheet stabilizes the C-terminus of chemerin in the TM binding pocket (CBR2) for receptor activation. The importance of GPR1 N-terminus in stabilizing chemerin binding is also evidenced by recent results using chimeric receptor-based binding assays [49]. At CBR2, contacts between the C-terminus of chemerin (C-terminal nonapeptides, structurally identical to C9 peptide) and CBR2 residues activate GPR1 downstream signaling. In some chemokine receptors, the receptor ECL2 form polar contacts with chemokine ligands, which defines a CRS3 [38]. Similar feature presents in chemerin-GPR1 interactions, where E109 at H2 helix of chemerin forms hydrogen bond with H194$^{5.26}$ of GPR1 close to ECL2 region. This region is therefore defined as CBR3 for chemerin binding. Canonical chemokine recognition sites involve a structurally conserved site 1.5 (CRS1.5), where the N-terminus of the receptor interacts with the CC/CXC motif of the chemokine [38,50]. This interaction, however, is absent in the chemerin-GPR1 complex. It is concluded that chemerin, which is not a chemokine, has retained some of the features that characterize the chemokine ligand-chemokine receptor interaction.

Our structural model also provides molecular insights into the mode of binding between the C-terminal nonapeptide of chemerin (C9) and GPR1, specifically at CBR2. C9 takes an "S"-shaped pose in the binding pocket of GPR1, which is surrounded by TM2, 3, 4, 6, and 7 and deep enough to accommodate the nonapeptide. The C-terminus of S9 reaches the bottom of the binding pocket and forms extensive polar interactions with S114$^{3.29}$, Q118$^{3.33}$, and R176$^{4.64}$. This model differs from the proposed model by Fischer and colleagues that was developed through homology modeling and molecular docking [44]. In the Fischer model, the C9-GPR1 interaction is dominated by hydrophobic interactions between F8 of the ligand and a hydrophobic domain in the extracellular loop 2 of GPR1 consisting of F$^{4.69}$, L$^{4.74}$, Y$^{4.76}$, and F$^{4.79}$. This feature, combined with a proposed hydrophobic interaction between F6 and F$^{2.68}$, renders a shallow hydrophobic pocket for ligand binding. For ligand accommodation in the Fischer model, the peptide ligand bent between G4 and Q5, pointing towards T$^{7.39}$, demonstrating a "U"-shaped pose. Apparently, the Fischer model is not energetically favorable for stable binding of the C-terminal peptide, which is critical to activation of the receptor for G protein signaling.

The binding poses of C9 and chemerin to GPR1 are similar, both adopting an "S"-shaped insertion into the TM pocket, but they exhibit subtle differences in the side chain orientations that result in distinct molecular interactions (S12 Fig). In the C9 peptide, the S9 residue bends upwards to form a polar contact with S114$^{3.29}$ of GPR1, while in chemerin, F136 rotates deeper into the hydrophobic cavity, contributing to its higher potency and efficacy (S12A Fig). Additionally, Y1 in C9 is oriented downwards closer to the TM pocket than Y129 in chemerin, correlating with a downward rotation of E269$^{6.58}$ in the C9-bound receptor, though the polar

interaction between Y1 (Y129 in chemerin) and E269$^{6.58}$ is maintained in both cases (S12B Fig).

Our structural model provides direct evidence for an interaction of GPR1 and the Gi proteins, which clarified an issue on whether GPR1 is able to signal through G proteins. Analysis of the receptor-Gi protein interface found some polar interactions between the receptor and G protein heterodimer complex. Of note, the highly conserved G protein-binding motif, D$^{3.49}$-R$^{3.50}$-Y$^{3.51}$, found in many Class A GPCRs, is replaced by DHY in GPR1. Surprisingly, histidine substitution in this motif did not diminish G protein binding. Notably, a polar interaction between H135$^{3.50}$ and G352 in the α5 helix of Gi is evident. This structural feature indicates that the canonical DRY motif is not absolutely necessary for GPCR-Gi interaction, and the actual coupling of the receptor to G protein may be context-specific in each of the receptors. However, as evidenced from our structural model, C-terminal end of the α5 helix is partially unfolded in GPR1. The modeling of D350 and C351 is also dampened by a limited local electron density. Altogether, the structural features at GPR1-Gi interface may explain for a weaker Gi activation by GPR1.

The chemerin/C9-bound GPR1-Gi signaling complex structure was compared with the C9-CMKLR1-Gi structure that we resolved earlier [24]. There are high degrees of homology at both primary sequence level (71% sequence similarity, with 37% identical amino acids) [4] and 3D structure level. For G protein interacting interface, CMKLR1 has additional polar interactions with the αN helix of Gαi than GPR1. The difference in DRY motif (DRC in CMKLR1, DHY in GPR1) does not seem to affect Gi coupling in pharmacological term. For the receptor-C9 interaction, the C9 peptide resumes an "S" shape in both GPR1 and CMKLR1. However, C9 insertion into the GPR1 binding pocket is not as deep as it is in CMKLR1, showing an average of 1.2 Å upward shift in GPR1. As a result, the bottom of the GPR1 binding pocket is higher above W$^{6.48}$, the "toggle switch" for G protein activation, when compared with CMKLR1 [24]. A more recent article on the structure of C9-CMKLR1-Gi complex highly coincides with our previously reported CMKLR1 structure, providing further cross-validation of our CMKLR1 and GPR1 structures [51]. Taken together, structural analysis of the GPR1-Gi signaling complex provides evidence that GPR1 is fully capable of activating Gi proteins despite minor sequence differences at the DRY motif and a shallower binding pocket for the peptide ligand.

While the structural information of GPR1 expands our knowledge in chemerin receptor biology, several unknowns still remain for further investigation. Given the high similarities between GPR1 and CMKLR1, they may share a variety of agonists and antagonists. Currently the only natural ligand of GPR1 and CMKLR1 is chemerin, and the wide distribution of GPR1 and CMKLR1 among immune cells, adipose tissues and central nervous system suggests the presence of other possible endogenous ligands [7,13,17]. Indeed, a previous report unraveled a novel ligand of GPR1, FAM19A1, which is highly expressed in adult hippocampus and has neural modulatory effect [52]. However, the reported study was based primarily on animal experiments without a biochemical mechanism for receptor activation, and there is still a lack of structural information about FAM19A1 interaction with GPR1. Another unresolved issue is whether GPR1 and CMKLR1 differ in activating the β-arrestin pathway, as currently there is a lack of structure for a ligand-bound receptor-β-arrestin complex. Further investigation in these directions will help to understand how the signals generated by chemerin binding are mediated by these 2 receptors.

Supporting information

S1 Fig. Protein purification, cryo-EM data collection, structure determination, and cryo-EM maps. (A) Size-exclusion chromatography elution profiles of the C9-GPR1-G protein

complex and the SDS–PAGE and Coomassie blue staining of the C9-GPR1-G protein complex. **(B)** Representative micrograph of the complex particles from 3,609 movies. **(C)** Representative 2D averages. **(D)** Workflow for cryo-EM image processing. **(E)** Gold standard Fourier shell correlation (FSC) curve indicates overall nominal resolution at 2.90 Å using the FSC = 0.143 criterion. **(F)** Local resolution map. The original gel image can be found in S1 Raw Images.
(TIFF)

S2 Fig. Protein purification, cryo-EM data collection, structure determination, and cryo-EM maps. (A) Size-exclusion chromatography elution profiles of the chemerin-GPR1-G protein complex and the SDS–PAGE and Coomassie blue staining of the chemerin-GPR1-G protein complex. **(B)** Representative micrograph of the complex particles from 7,706 movies. **(C)** Representative 2D averages. **(D)** Workflow for cryo-EM image processing. **(E)** Gold standard Fourier shell correlation (FSC) curve indicates overall nominal resolution at 3.29 Å using the FSC = 0.143 criterion. **(F)** Local resolution map. The original gel image can be found in S1 Raw Images.
(TIFF)

S3 Fig. Representative density maps and models for TM1-7 and H8 of GPR1 and C-terminal α helices of Gαi1 (α5 and αN) and the ligand C9 peptide.
(TIFF)

S4 Fig. Cell surface expression of mutants. HEK293T cells were transfected with FLAG-tagged WT or mutant GPR1 for 24 h at 37˚C. The cells were then incubated with an FITC-conjugated FLAG antibody for 30 min on ice. The fluorescence signals on the cell surface were quantified by flow cytometry. Data shown are means ± SEM from 3 independent experiments. *, $p < 0.05$. The underlying data can be found in S1 Data.
(TIFF)

S5 Fig. Backbone RMSD of the full-length (upper panel) and TM helices (lower panel) of GPR1 in each replica of MD simulation. The underlying data can be found in S1 Data.
(TIFF)

S6 Fig. The hydrophobic contact analysis of the C9 peptide binding on GPR1. (A) The average heavy-atom distance of close-contact residues between C9 and GPR1. **(B, C)** The relative distribution of the close-contact residues around the C9 peptide. The underlying data can be found in S1 Data.
(TIFF)

S7 Fig. 2D free energy map of the C9 unbinding from GPR1 pocket. The experimental conformation is marked by red cross on the map. The underlying data can be found in S1 Data.
(TIFF)

S8 Fig. Time evolution of the Z-component of C9-GPR1 distance. The underlying data can be found in S1 Data.
(TIFF)

S9 Fig. Time evolution of the Z-component of full length chemerin-GPR1 distance. The underlying data can be found in S1 Data.
(TIFF)

S10 Fig. Comparison of the ligand binding pocket of GPR1 (marine blue) and CMKLR1 (cyan). (A) Sphere representation of C9 bound to GPR1 is shown in orange, and the C9

bound to CMKLR1 is shown in magenta. $W^{6.48}$ "toggle switch" is highlighted with stick representation. **(B)** Key interaction residues of the binding pockets of GPR1 and CMKLR1 are shown in licorice representation. The ligands respectively bound to the 2 receptors are shown as ribbon. The distance of the ligands is calculated and shown as a centroid distance of 1.2 Å.
(TIFF)

S11 Fig. Comparison of structural motifs for G protein activation between GPR1 (dark blue) and CMKLR1 (cyan). The residues responsible for G protein activation are highlighted in sticks. The G protein in the GPR1-Gi structure is shown in magenta, and the G protein in the CMKLR1-Gi structure is shown in light pink.
(TIFF)

S12 Fig. Comparison of molecular interactions between chemerin (lime green)-bound GPR1 (cyan) and C9 (orange)-bound GPR1 (purple). GPR1 residues for polar contacts with the 2 ligands are highlighted in sticks. Side chain conformational changes are indicated with red arrows.
(TIFF)

S1 Table. Cryo-EM data collection, model refinement, and validation statistics.
(TIFF)

S1 Raw Images. The raw SDS-PAGE data for SDS-PAGE images in S1A and S2A Fig, showing the concentrated protein samples of C9-GPR1-Gi-scFv16 complex and chemerin-GPR1-Gi-scFv16 complex, respectively.
(PDF)

S1 Data. The raw data for Figs 1A–1D, 2F-2I, 4C-4F, 9A-9F, and S4–S9. Additionally, raw MD simulation data for Figs 6 and S5–S9 can be accessed in https://doi.org/10.5281/zenodo.13711859.
(XLSX)

Acknowledgments

The authors thank the Kobilka Cryo-Electron Microscopy Center in the Chinese University of Hong Kong, Shenzhen, for cryo-electron microscopy analysis, and their technicians for kind help and technical support. The authors thank the Warshel Institute for Computational Biology (funding from Shenzhen City and Longgang District) for computational work.

Author Contributions

Conceptualization: Aijun Liu, Yezhou Liu, Richard D. Ye.

Data curation: Aijun Liu, Yezhou Liu, Geng Chen, Wenping Lyu.

Funding acquisition: Aijun Liu, Lizhe Zhu, Yang Du, Richard D. Ye.

Investigation: Aijun Liu, Yezhou Liu, Geng Chen, Wenping Lyu, Fang Ye, Junlin Wang, Qiwen Liao.

Methodology: Aijun Liu, Yezhou Liu, Wenping Lyu.

Supervision: Lizhe Zhu, Yang Du, Richard D. Ye.

Validation: Aijun Liu, Yezhou Liu, Richard D. Ye.

Visualization: Aijun Liu, Yezhou Liu, Wenping Lyu.

Writing – original draft: Aijun Liu, Yezhou Liu, Richard D. Ye.

Writing – review & editing: Aijun Liu, Yezhou Liu, Richard D. Ye.

References

1. Goralski KB, McCarthy TC, Hanniman EA, Zabel BA, Butcher EC, Parlee SD, et al. Chemerin, a novel adipokine that regulates adipogenesis and adipocyte metabolism. J Biol Chem. 2007; 282(38):28175–28188. Epub 20070716. https://doi.org/10.1074/jbc.M700793200 PMID: 17635925.
2. Bozaoglu K, Bolton K, McMillan J, Zimmet P, Jowett J, Collier G, et al. Chemerin is a novel adipokine associated with obesity and metabolic syndrome. Endocrinology. 2007; 148(10):4687–4694. Epub 20070719. https://doi.org/10.1210/en.2007-0175 PMID: 17640997.
3. Lehrke M, Becker A, Greif M, Stark R, Laubender RP, von Ziegler F, et al. Chemerin is associated with markers of inflammation and components of the metabolic syndrome but does not predict coronary atherosclerosis. Eur J Endocrinol. 2009; 161(2):339–344. Epub 20090604. https://doi.org/10.1530/EJE-09-0380 PMID: 19497986.
4. Kennedy AJ, Davenport AP. International Union of Basic and Clinical Pharmacology CIII: Chemerin Receptors CMKLR1 (Chemerin1) and GPR1 (Chemerin2) Nomenclature, Pharmacology, and Function. Pharmacol Rev. 2018; 70(1):174–196. Epub 20171226. https://doi.org/10.1124/pr.116.013177 PMID: 29279348.
5. Helfer G, Wu QF. Chemerin: a multifaceted adipokine involved in metabolic disorders. J Endocrinol. 2018; 238(2):R79–R94. Epub 20180530. https://doi.org/10.1530/JOE-18-0174 PMID: 29848608.
6. Goralski KB, Jackson AE, McKeown BT, Sinal CJ. More Than an Adipokine: The Complex Roles of Chemerin Signaling in Cancer. Int J Mol Sci. 2019; 20(19). Epub 20190926. https://doi.org/10.3390/ijms20194778 PMID: 31561459.
7. Wittamer V, Franssen JD, Vulcano M, Mirjolet JF, Le Poul E, Migeotte I, et al. Specific recruitment of antigen-presenting cells by chemerin, a novel processed ligand from human inflammatory fluids. J Exp Med. 2003; 198(7):977–985. https://doi.org/10.1084/jem.20030382 PMID: 14530373.
8. Meder W, Wendland M, Busmann A, Kutzleb C, Spodsberg N, John H, et al. Characterization of human circulating TIG2 as a ligand for the orphan receptor ChemR23. FEBS Lett. 2003; 555(3):495–499. https://doi.org/10.1016/s0014-5793(03)01312-7 PMID: 14675762.
9. Zabel BA, Silverio AM, Butcher EC. Chemokine-like receptor 1 expression and chemerin-directed chemotaxis distinguish plasmacytoid from myeloid dendritic cells in human blood. J Immunol. 2005; 174(1):244–251. https://doi.org/10.4049/jimmunol.174.1.244 PMID: 15611246.
10. Zabel BA, Allen SJ, Kulig P, Allen JA, Cichy J, Handel TM, et al. Chemerin activation by serine proteases of the coagulation, fibrinolytic, and inflammatory cascades. J Biol Chem. 2005; 280(41):34661–34666. Epub 20050811. https://doi.org/10.1074/jbc.M504868200 PMID: 16096270.
11. Zabel BA, Nakae S, Zuniga L, Kim JY, Ohyama T, Alt C, et al. Mast cell-expressed orphan receptor CCRL2 binds chemerin and is required for optimal induction of IgE-mediated passive cutaneous anaphylaxis. J Exp Med. 2008; 205(10):2207–2220. Epub 20080915. https://doi.org/10.1084/jem.20080300 PMID: 18794339.
12. Barnea G, Strapps W, Herrada G, Berman Y, Ong J, Kloss B, et al. The genetic design of signaling cascades to record receptor activation. Proc Natl Acad Sci U S A. 2008; 105(1):64–69. Epub 20071228. https://doi.org/10.1073/pnas.0710487105 PMID: 18165312.
13. Marchese A, Docherty JM, Nguyen T, Heiber M, Cheng R, Heng HH, et al. Cloning of human genes encoding novel G protein-coupled receptors. Genomics. 1994; 23(3):609–618. https://doi.org/10.1006/geno.1994.1549 PMID: 7851889.
14. De Henau O, Degroot GN, Imbault V, Robert V, De Poorter C, McHeik S, et al. Signaling Properties of Chemerin Receptors CMKLR1, GPR1 and CCRL2. PLoS ONE. 2016; 11(10):e0164179. Epub 20161007. https://doi.org/10.1371/journal.pone.0164179 PMID: 27716822.
15. Rourke JL, Dranse HJ, Sinal CJ. CMKLR1 and GPR1 mediate chemerin signaling through the RhoA/ROCK pathway. Mol Cell Endocrinol. 2015; 417:36–51. Epub 20150909. https://doi.org/10.1016/j.mce.2015.09.002 PMID: 26363224.
16. Samson M, Edinger AL, Stordeur P, Rucker J, Verhasselt V, Sharron M, et al. ChemR23, a putative chemoattractant receptor, is expressed in monocyte-derived dendritic cells and macrophages and is a coreceptor for SIV and some primary HIV-1 strains. Eur J Immunol. 1998; 28(5):1689–1700. https://doi.org/10.1002/(SICI)1521-4141(199805)28:05<1689::AID-IMMU1689>3.0.CO;2-I PMID: 9603476.
17. Tokizawa S, Shimizu N, Hui-Yu L, Deyu F, Haraguchi Y, Oite T, et al. Infection of mesangial cells with HIV and SIV: identification of GPR1 as a coreceptor. Kidney Int. 2000; 58(2):607–617. https://doi.org/10.1046/j.1523-1755.2000.00207.x PMID: 10916084.

18. Shimizu N, Tanaka A, Oue A, Mori T, Ohtsuki T, Apichartpiyakul C, et al. Broad usage spectrum of G protein-coupled receptors as coreceptors by primary isolates of HIV. AIDS. 2009; 23(7):761–769. https://doi.org/10.1097/QAD.0b013e328326cc0d PMID: 19307942.

19. Rourke JL, Muruganandan S, Dranse HJ, McMullen NM, Sinal CJ. Gpr1 is an active chemerin receptor influencing glucose homeostasis in obese mice. J Endocrinol. 2014; 222(2):201–215. Epub 20140603. https://doi.org/10.1530/JOE-14-0069 PMID: 24895415.

20. Ernst MC, Sinal CJ. Chemerin: at the crossroads of inflammation and obesity. Trends Endocrinol Metab. 2010; 21(11):660–667. https://doi.org/10.1016/j.tem.2010.08.001 PMID: 20817486.

21. Neves KB, Nguyen Dinh Cat A, Alves-Lopes R, Harvey KY, Costa RMD, Lobato NS, et al. Chemerin receptor blockade improves vascular function in diabetic obese mice via redox-sensitive and Akt-dependent pathways. Am J Physiol Heart Circ Physiol. 2018; 315(6):H1851–H1860. Epub 20180914. https://doi.org/10.1152/ajpheart.00285.2018 PMID: 30216119.

22. Karagiannis GS, Weile J, Bader GD, Minta J. Integrative pathway dissection of molecular mechanisms of moxLDL-induced vascular smooth muscle phenotype transformation. BMC Cardiovasc Disord. 2013; 13:4. Epub 20130116. https://doi.org/10.1186/1471-2261-13-4 PMID: 23324130.

23. Caulfield M, Munroe P, Pembroke J, Samani N, Dominiczak A, Brown M, et al. Genome-wide mapping of human loci for essential hypertension. Lancet. 2003; 361(9375):2118–2123. https://doi.org/10.1016/S0140-6736(03)13722-1 PMID: 12826435.

24. Wang J, Chen G, Liao Q, Lyu W, Liu A, Zhu L, et al. Cryo-EM structure of the human chemerin receptor 1-Gi protein complex bound to the C-terminal nonapeptide of chemerin. Proc Natl Acad Sci U S A. 2023; 120(11):e2214324120. Epub 20230307. https://doi.org/10.1073/pnas.2214324120 PMID: 36881626.

25. Chun E, Thompson AA, Liu W, Roth CB, Griffith MT, Katritch V, et al. Fusion partner toolchest for the stabilization and crystallization of G protein-coupled receptors. Structure. 2012; 20(6):967–976. https://doi.org/10.1016/j.str.2012.04.010 PMID: 22681902.

26. Chen G, Wang X, Liao Q, Ge Y, Jiao H, Chen Q, et al. Structural basis for recognition of N-formyl peptides as pathogen-associated molecular patterns. Nat Commun. 2022; 13(1):5232. Epub 20220905. https://doi.org/10.1038/s41467-022-32822-y PMID: 36064945.

27. Anandakrishnan R, Aguilar B, Onufriev AV. H++ 3.0: automating pK prediction and the preparation of biomolecular structures for atomistic molecular modeling and simulations. Nucleic Acids Res. 2012; 40 (Web Server issue):W537–W541. Epub 20120508. https://doi.org/10.1093/nar/gks375 PMID: 22570416.

28. Huang J, Rauscher S, Nawrocki G, Ran T, Feig M, de Groot BL, et al. CHARMM36m: an improved force field for folded and intrinsically disordered proteins. Nat Methods. 2017; 14(1):71–73. Epub 20161107. https://doi.org/10.1038/nmeth.4067 PMID: 27819658.

29. Pfaendtner J, Bonomi M. Efficient Sampling of High-Dimensional Free-Energy Landscapes with Parallel Bias Metadynamics. J Chem Theory Comput. 2015; 11(11):5062–5067. Epub 20151009. https://doi.org/10.1021/acs.jctc.5b00846 PMID: 26574304.

30. Inoue A, Raimondi F, Kadji FMN, Singh G, Kishi T, Uwamizu A, et al. Illuminating G-Protein-Coupling Selectivity of GPCRs. Cell. 2019; 177(7):1933–1947 e25. Epub 20190531. https://doi.org/10.1016/j.cell.2019.04.044 PMID: 31160049.

31. Maeda S, Koehl A, Matile H, Hu H, Hilger D, Schertler GFX, et al. Development of an antibody fragment that stabilizes GPCR/G-protein complexes. Nat Commun. 2018; 9(1):3712. Epub 2018/09/15. https://doi.org/10.1038/s41467-018-06002-w PMID: 30213947.

32. Ballesteros JA, Weinstein H. Integrated methods for the construction of three-dimensional models and computational probing of structure-function relations in G protein-coupled receptors. Methods Neurosci. 1995; 25:366–428.

33. Zhuang Y, Liu H, Edward Zhou X, Kumar Verma R, de Waal PW, Jang W, et al. Structure of formylpeptide receptor 2-Gi complex reveals insights into ligand recognition and signaling. Nat Commun. 2020; 11(1):885. Epub 2020/02/16. https://doi.org/10.1038/s41467-020-14728-9 PMID: 32060286.

34. Chen T, Xiong M, Zong X, Ge Y, Zhang H, Wang M, et al. Structural basis of ligand binding modes at the human formyl peptide receptor 2. Nat Commun. 2020; 11(1):1208. Epub 2020/03/07. https://doi.org/10.1038/s41467-020-15009-1 PMID: 32139677.

35. Zhu Y, Lin X, Zong X, Han S, Wang M, Su Y, et al. Structural basis of FPR2 in recognition of Abeta42 and neuroprotection by humanin. Nat Commun. 2022; 13(1):1775. Epub 20220401. https://doi.org/10.1038/s41467-022-29361-x PMID: 35365641.

36. Zhuang Y, Wang L, Guo J, Sun D, Wang Y, Liu W, et al. Molecular recognition of formylpeptides and diverse agonists by the formylpeptide receptors FPR1 and FPR2. Nat Commun. 2022; 13(1):1054. Epub 20220225. https://doi.org/10.1038/s41467-022-28586-0 PMID: 35217703.

37. Wittamer V, Gregoire F, Robberecht P, Vassart G, Communi D, Parmentier M. The C-terminal nonapeptide of mature chemerin activates the chemerin receptor with low nanomolar potency. J Biol Chem. 2004; 279(11):9956–9962. Epub 20031229. https://doi.org/10.1074/jbc.M313016200 PMID: 14701797.

38. Urvas L, Kellenberger E. Structural Insights into Molecular Recognition and Receptor Activation in Chemokine-Chemokine Receptor Complexes. J Med Chem. 2023; 66(11):7070–7085. Epub 20230522. https://doi.org/10.1021/acs.jmedchem.3c00352 PMID: 37212620.

39. Kufareva I, Gustavsson M, Zheng Y, Stephens BS, Handel TM. What Do Structures Tell Us About Chemokine Receptor Function and Antagonism? Annu Rev Biophys. 2017; 46:175–198. https://doi.org/10.1146/annurev-biophys-051013-022942 PMID: 28532213.

40. Weis WI, Kobilka BK. The Molecular Basis of G Protein-Coupled Receptor Activation. Annu Rev Biochem. 2018; 87:897–919. https://doi.org/10.1146/annurev-biochem-060614-033910 PMID: 29925258.

41. Zhou Q, Yang D, Wu M, Guo Y, Guo W, Zhong L, et al. Common activation mechanism of class A GPCRs. Elife. 2019;8. Epub 20191219. https://doi.org/10.7554/eLife.50279 PMID: 31855179.

42. Lee E, Taussig R, Gilman AG. The G226A mutant of Gs alpha highlights the requirement for dissociation of G protein subunits. J Biol Chem. 1992; 267(2):1212–1218. PMID: 1730644.

43. Posner BA, Mixon MB, Wall MA, Sprang SR, Gilman AG. The A326S mutant of Gialpha1 as an approximation of the receptor-bound state. J Biol Chem. 1998; 273(34):21752–21758. https://doi.org/10.1074/jbc.273.34.21752 PMID: 9705312.

44. Fischer TF, Czerniak AS, Weiß T, Schoeder CT, Wolf P, Seitz O, et al. Ligand-binding and -scavenging of the chemerin receptor GPR1. Cell Mol Life Sci. 2021; 78(17–18):6265–6281. https://doi.org/10.1007/s00018-021-03894-8 PMID: 34241650

45. Degroot GN, Lepage V, Parmentier M, Springael JY. The Atypical Chemerin Receptor GPR1 Displays Different Modes of Interaction with beta-Arrestins in Humans and Mice with Important Consequences on Subcellular Localization and Trafficking. Cells. 2022; 11(6). Epub 20220318. https://doi.org/10.3390/cells11061037 PMID: 35326488.

46. Zabel BA, Zuniga L, Ohyama T, Allen SJ, Cichy J, Handel TM, et al. Chemoattractants, extracellular proteases, and the integrated host defense response. Exp Hematol. 2006; 34(8):1021–1032. https://doi.org/10.1016/j.exphem.2006.05.003 PMID: 16863908.

47. Kumar JD, Aolymat I, Tiszlavicz L, Reisz Z, Garalla HM, Beynon R, et al. Chemerin acts via CMKLR1 and GPR1 to stimulate migration and invasion of gastric cancer cells: putative role of decreased TIMP-1 and TIMP-2. Oncotarget. 2019; 10(2):98–112. Epub 20190104. https://doi.org/10.18632/oncotarget.26414 PMID: 30719206.

48. Siciliano SJ, Rollins TE, DeMartino J, Konteatis Z, Malkowitz L, Van Riper G, et al. Two-site binding of C5a by its receptor: an alternative binding paradigm for G protein-coupled receptors. Proc Natl Acad Sci U S A. 1994; 91(4):1214–1218. https://doi.org/10.1073/pnas.91.4.1214 PMID: 8108389.

49. Kretschmer K, Zellmann T, Morl K, Beck-Sickinger AG. Stable Binding of Full-Length Chemerin Is Driven by Negative Charges in the CMKLR1 N Terminus. Chembiochem. 2023; 24(18):e202300280. Epub 20230809. https://doi.org/10.1002/cbic.202300280 PMID: 37186779.

50. Kleist AB, Getschman AE, Ziarek JJ, Nevins AM, Gauthier PA, Chevigne A, et al. New paradigms in chemokine receptor signal transduction: Moving beyond the two-site model. Biochem Pharmacol. 2016; 114:53–68. Epub 20160419. https://doi.org/10.1016/j.bcp.2016.04.007 PMID: 27106080.

51. Zhang X, Weiß T, Cheng MH, Chen S, Ambrosius CK, Czerniak AS, et al. Structural basis of G protein-Coupled receptor CMKLR1 activation and signaling induced by a chemerin-derived agonist. PLoS Biol. 2023; 21(12):e3002188. Epub 20231206. https://doi.org/10.1371/journal.pbio.3002188 PMID: 38055679.

52. Zheng C, Chen D, Zhang Y, Bai Y, Huang S, Zheng D, et al. FAM19A1 is a new ligand for GPR1 that modulates neural stem-cell proliferation and differentiation. FASEB J. 2018:fj201800020RRR. Epub 20180525. https://doi.org/10.1096/fj.201800020RRR PMID: 29799787.